ABSTRACT

Title of Thesis: MODELING VISCOELASTIC BEHAVIOR USING FLEXIBLE MULTIBODY DYNAMICS FORMULATIONS

Nishant Nemani
Master of Science, 2020

Thesis Directed by: Professor Olivier Bauchau
Department of Aerospace Engineering

Viscoelastic behavior is frequently observed in dynamical flexible multibody systems. In the simplest form it is manifested in one dimensional revolute and prismatic joints. Beyond which more complex force elements such as six degree of freedom flexible joints can also be found. Finally, beams, plates and shells are found to exhibit viscoelastic behavior too. In the past extensive work has been done on analyzing the dynamic response of three dimensional beams by performing cross-sectional analysis through finite element methods and subsequently solving the reduced beam problem. The approach is particularly relevant for the analysis of complex cross sections and helps improve computational efficiency significantly. A formulation which incorporates a viscoelastic model of the generalized Maxwell type with a solution of the three dimensional beam theory which gives an exact solution of static three dimensional elasticity problems is presented. Multiple examples incorporating the use of the aforementioned model in the context of viscoelastic beams and joints are presented. Shortcomings of the Kelvin-Voigt model, which is

often used for flexible multibody systems, are underlined.

MODELLING VISCOELASTIC BEEHAVIOR USING FLEXIBLE MULTIBODY DYNAMICS FORMULATIONS

by

Nishant Nemani

Thesis submitted to the Faculty of the Graduate School of the
University of Maryland, College Park in partial fulfillment
of the requirements for the degree of
Master of Science
2020

Advisory Committee:
Professor Olivier A. Bauchau, Chair/Advisor
Professor Sung Lee
Professor Anubhav Datta

Acknowledgments

First and foremost, I would like to thank Prof. Olivier Bauchau for his consistent and patient guidance throughout my time as a student at the University of Maryland. I am incredible grateful for the opportunity to be able to learn from him over these past few years.

I would also like to thank Prof. Lee and Prof. Datta for their advice and support as my committee members.

I am also thankful to my parents and my sister for always encouraging and supporting me in my academic pursuits and for their moral support in difficult times.

I would also like to thank current and former members of our research group Valentin, Alfonso, Shilei, Tyler, Giuseppe, Matteo, Minghe, Ray & Andrew. I have been fortunate to learn a lot from them and I am extremely grateful for the support they have extended as collegues. I will always remember our group lunches fondly.

Last but not the least, I would like to thank all the members of the Caladrius design team, Seyhan, Ravi, Shashank, Mrinal, Abhishek and Amy and our faculty advisors Prof. Chopra and Dr. Nagaraj for their guidance throughout the semester. Being on the team was truly one of the great experiences of my life.

Table of Contents

List of Tables

List of Figures

List of Abbreviations

M.F.	Maxwell Fluid
PDE	Partial differential equation
NREL	National Renewable Energy Laboratory
EB	Euler-Bernoulli

Chapter 1: Introduction

1.1 Literature Review

A beam is a structural element whose cross-sectional dimensions are much smaller than the length of the element. The area of solid mechanics which specifically deal with the behaviour of beams is known as beam theory. For beam problems a number of theories have been proposed, depending on the nature of the problem that is required to be solved. We are looking to deal with beams having complex cross sections. Such beams are commonly observed in the case of rotor craft, like helicopters, wind turbines etc. In such beams viscoelastic damping due to the nature of materials that are used can be observed. While a full fledged three dimensional finite element analysis can be performed for the same it is much more expensive computationally. Especially during early design stages, it is useful to have reduced models for analyzing various structural components. The analysis of complex cross sections in linear elastic beams was first done by Giavotto et al. [1]. The approach presented a formulation to relate the sectional strains and curvatures with the sectional forces and moments using a sectional stiffness matrix. The sectional strains and curvatures can be used to recover the three dimensional stresses across the beam. Simo et al. [2] formulated sectional-level visco-plastic constitutive laws for

geometrically exact rods without resorting to local, three dimensional constitutive laws. Mata et al. [3] developed a nonlinear constitutive model for the analysis of the dynamic behavious of beams based on the formulation by Simo [4]. They introduced viscoelasticity in the material model by incorporating it in the first Piola-Kirchhoff stress tensor. In the paper by Abdel-Nasser and Shabana [5] viscous damping was incorporated using a three dimensional Kelvin-Voigt model into a geometrically nonlinear beam formulation using absolute nodal co-ordinates. The formulation was was inapplicable to incompressible materials and was seen to suffer from Poisson locking. A Kelvin-Voigt model was also proposed by Antman [6] as a source of numerical dissipation overcome problems of shock wave formation in the undamped, nonlinear coupled system of PDEs in Cosserat rods. Ribe [7] studied the coiling of fluid flows, the coiling was found to be fundamentally similar to simultaneous folding of viscous sheets and coiling of an elastic rope. It was shown that the three dimensional Navier-Stokes equations for fluid flow could be reduced to the dynamic equilibrium equations of a Kirchhoff/Love rod having a Maxwell type constitutive equation for the viscous forces and moments. An incompressible fluid flow model was used to model the extensional flow of the fluid with lateral contraction where the experimental findings from Trouton [8] on the shear and extensional viscosity being η and 3η respectively were incorporated. Extensions to the work done by Ribe [7] can be found in Panda et al. [9] who presented a asymptotic model to describe the spinning of a slender curved inertial viscous Newtonian fiber with a free boundary condition at the end. Marheineke and Wegener [10] further generalized the model presented in [9] by incorporating the effect of surface tension and deducing the boundary con-

dition for the free end. Klar et al. [11] and Arne et al. [12] developed a furmulation for the simulation of viscous fiber for the application to woven and unwoven textiles using Ribe's Maxwell-type constitutive laws. Lang et al. [13] used a Cosserat rod model to simulate a the dynamical behavior of viscoelastic rods with quaternions being used to parameterize rotations. In these formulations the sectional stiffness matrix is used to relate the sectional stresses to the sectional strains. Additionally, viscous stress resultants were introduced which were considered to be proportional to the sectional strain rates using effective damping parameters. The model prescribed in this paper was used to simulate the 5MW NREL wind turbine by Schulze et al. [14] trough a fully integrated multibody dynamics formulation. Lang et al. [15] also used the model detailed in [13] to study both purely viscous and fully dynamic effects. Critical values of shear and extensional viscosity were evaluated and were later used to damp out the unwanted high frequency modes in fully nonlinear computations. Finally Linn et al. [16] added Kelvin-Voigt type viscous damping to the Cosserat rod model for homogeneous and isotropic materials. It was observed that a slight damping of oscillation amplitudes can be seen for a clamped cantilever beam. Cross sectional warping deformation was neglected for their study and the damping parameters were corrected in an ad-hoc manner as per Cowper [17]. Due to the limitations imposed on the model they could not be extended to complex cross sections or more complex viscoelastic models like the generalized Maxwell model. The aim of this paper is to incorporate the well known generalized Maxwell model for viscoelasticity with already existing beam theories. A detailed formulation of the the solution techniques employed for viscoelastic beams is presented. It can be

easily extended to elements like elastomeric dampers and flexible joints made out of viscoelastic material, numerical examples for both are presented.

Chapter 2: Review of Classical Viscoelasticity

Viscoelastic behavior is commonly represented with the help of springs and dashpots associated in a variety of ways. Using different combinations a variety of viscoelastic models can be represented. For a detailed presentation of viscoelastic constitutive laws the reader is referred to Flügge [18]. Our work is limited to the application of the generalized Maxwell model for viscoelasticity. It will be briefly discussed in this section.

2.1 The Generalized Maxwell model

In all models the springs are used to represent the elastic behavior of the material while dashpots are used to characterize the energy dissipation in the material. The generalized Maxwell model consists of an elastic branch coupled with one or more Maxwell fluid branches in parallel. A Maxwell fluid branch is simply a combination of an elastic spring and a dashpot connected in series. A Zener model one where the elastic branch is coupled with one Maxwell fluid branch. A schematic model of the generalized Maxwell model is presented in fig. 2.1.

The elastic branch has a Young's modulus E_∞ while the springs in the Maxwell fluid branches have a Young's modulus E_n. The stresses in the elastic springs in

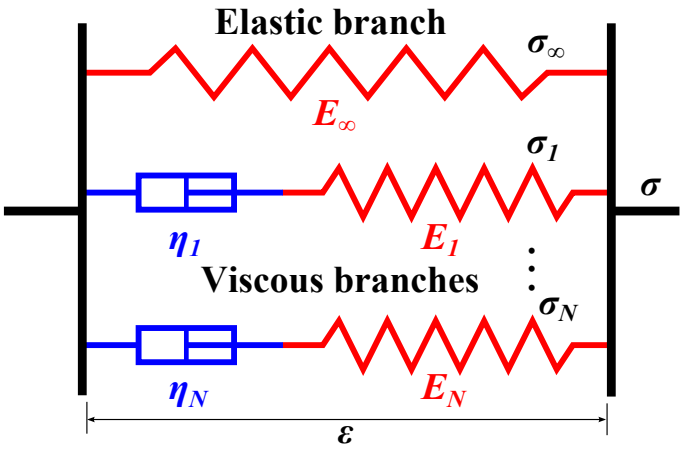

Fig. 2.1: Schematic representation of a generalized Maxwell model.

the Maxwell fluid branches can be given as $\sigma_n = E_n\epsilon_n$. An internal state parameter α_n is associated with each dashpot and this gives the strain in the elastic springs as $\epsilon_n = \epsilon - \alpha_n$. The total stress in the Maxwell Model is given as

$$\sigma = E_\infty\epsilon + \sum_{n=1}^{N} E_n(\epsilon - \alpha_n) \tag{2.1}$$

Each Maxwell fluid element is also associated with a relaxation time, $\tau_n = \eta_n/E_n$. The relaxation time relates the internal state parameters of the dashpots with the total stain in the element given as

$$\tau_n\dot{\alpha}_n + \alpha_n = \epsilon \tag{2.2}$$

The evolution equation can be recast in differential form as $d[e^{(t/\tau_n)}\alpha_n]/dt = (1/\tau_n)e^{(t/\tau_n)}\epsilon$, which can be expressed in the form of a convolution integral $\alpha_n(t) = (1/\tau_n)\int_{-\infty}^{t} e^{-(t-s)/\tau_n}\epsilon(s)ds$. On integration by parts we have

$$\alpha_n(t) = \epsilon(t) - \int_{-\infty}^{t} e^{\frac{-(t-s)}{\tau_n}} \dot{\epsilon}(s) ds \tag{2.3}$$

Which leads to a stress convolution integral consisting of a relaxation function, $G(t)$ given as

$$\sigma_n(t) = \int_{-\infty}^{t} G(t-s)\dot{\epsilon}(s) ds \tag{2.4}$$

$$G(t) = E_\infty + \sum_{n=1}^{N} E_n e^{(-t/\tau_n)} \tag{2.5}$$

Clearly, in the absence of viscoelasticity, when either E_n or τ_n vanish, linearly elastic constitutive relations can be recovered from the above expression. In the special case where a periodic strain is applied to the viscoelastic material another commonly accepted way to represent viscoelasticity relations is in the frequency domain in terms of the storage and loss modulus. The strain can be replaced with $\epsilon = \epsilon_0 e^{i\omega t}$, which gives us a stress-strain relation of the form

$$\sigma(t) = (E_\infty + \sum_{n=1}^{N} E_n \frac{i\omega\tau_n}{1 + i\omega\tau_n})\epsilon(t) \tag{2.6}$$

The viscoelastic modulus in this case can be separated into the storage and the loss moduli, G_s and G_l, which are given as

$$\sigma(t) = (G_s(\omega) + iG_l(\omega))\epsilon(t) \tag{2.7}$$

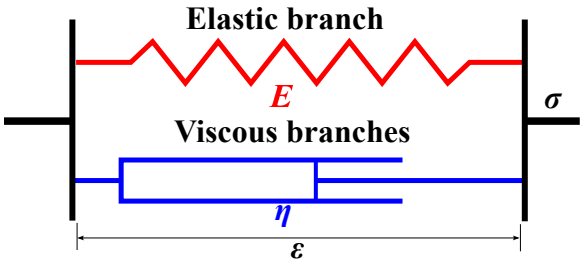

Fig. 2.2: Kelvin-Voigt model

$$G_s(\omega) = E_\infty + \sum_{n=1}^{N} E_n \frac{(\omega\tau_n)^2}{1 + (\omega\tau_n)^2} \tag{2.8}$$

$$G_l(\omega) = \sum_{n=1}^{N} E_n \frac{\omega\tau_n}{1 + (\omega\tau_n)^2} \tag{2.9}$$

Clearly, we can say that the resulting stress is going to have a phase difference with the strain. The component of the stress which is in phase with the applied strain is defined using the storage modulus while the component of the stress that is out of phase with the strain is prescribed using the loss modulus. The phase difference between the stress and the strain can be given as $\delta = arctan(G_l/G_s)$. For a more detailed presentation the reader is referred to Ferry [19].

2.2 Why Generalized Maxwell model?

In the past researchers have extensively used the Kelvin-Voigt model for modeling viscoelastic materials. However, there is a shortcoming that has not been accounted for. The Kelvin-Voigt model, as shown in fig. 2.2, is a special case of a Generalized Maxwell model with The following properties $N_b = 1$, $E_\infty = E$, $\tau_1 = 0$ and $E_1 \to \infty$. This results in an increasing non-dimensional loss modulus,

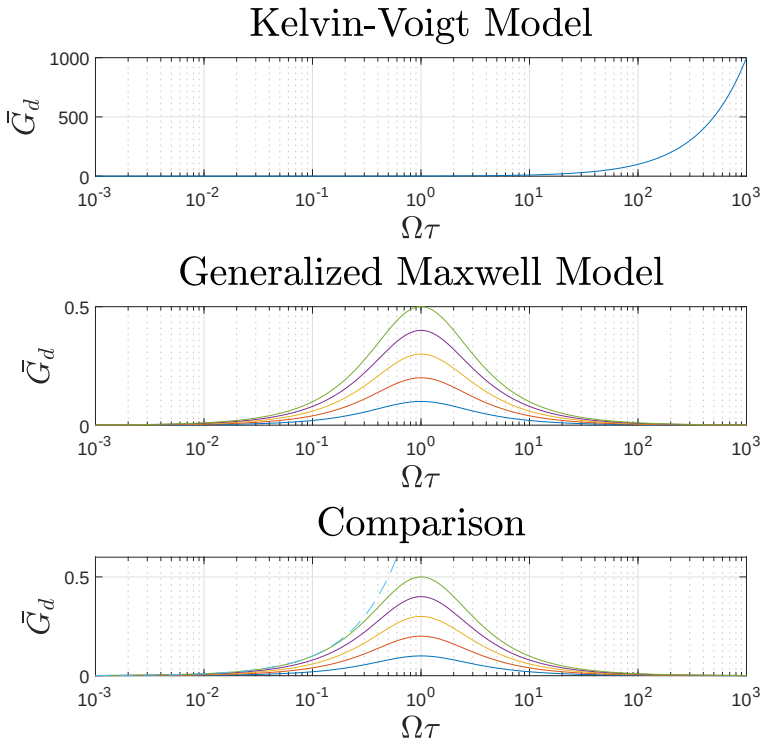

Fig. 2.3: Loss modulus as a function of non dimensional frequency. In the comparison '—' is for the Generalized Maxwell model and '- -' is for the Kelvin-Voigt model

$\bar{G}_d = G_d/(E_\infty + E_1)$, with an increasing non-dimensional frequency as shown in fig. 2.3. This is unreasonable because normally materials are not found to dissipate large amounts of energy at high excitation frequencies. On the other hand, trends for the Generalized Maxwell model are more realistic. The non-dimensional loss modulus is seen to increase with increasing excitation frequency until it reaches a peak, thereafter it tapers off asymptotically as shown in fig. 2.3. For the Generalized Maxwell model the non-dimensional loss modulus varies depending on the ratio $E_1/(E_\infty + E_1)$. This results in multiple plots for the Generalized Maxwell case. A comparison of the Kelvin-Voigt and Generalized Maxwell model is presented in the bottommost polt. We find that the Kelvin-Voigt model indeed increases at a faster

rate than the Generalized-Maxwell model.

Chapter 3: Beam Theory

The viscoelastic formulation presented in this paper are based on the three-dimensional beam theory developed by Baucahu and Han [20]. The 3-D beam theory is used to reduce the problem of analyzing a fully three dimensional beam into an equivalent one dimensional beam where all the 3D stress and strain states can be recovered and the warping deformations are accounted for. The beam theory provides an exact solution of the static Saint-Venant problem. This has some important implications. It is assumed that the beam has infinite length and is loaded at the ends. The cross- section to be analyzed itself, should be sufficiently far away from the boundaries to avoid end effects. The warping displacements and strains are assumed to remain small. The cross-section itself can be composed of heterogeneous and anisotropic materials. Their formulation used a Hamiltonian formalism to obtain the solution of the St. Venant problem. The formulation of this beam theory is presented in this chapter.

3.1 Kinematics

A typical beam cross sectional setup for our problem is shown in fig. 3.1. An arbitrarily twisted beam, of length L and cross sectional area A is considered. A

curve $\mathcal{C}$ can be prescribed as a reference line passing through the center of the beam's cross section at every location. An intrinsic parameterization of the curve is defined as α_1 and a unit tangent vector to the curve $\mathcal{C}$, is found as $\bar{t} = \partial \underline{r}_B / \partial \alpha_1$, where $\underline{r}_B$ defines the position of center of a given cross section of the beam defined in the inertial frame of reference $\mathcal{F} = [\mathbf{O}, \mathcal{I} = (\bar{\imath}_1, \bar{\imath}_2, \bar{\imath}_3)]$. In the reference frame for the undeformed beam cross sections are defined as $\mathcal{F}^* = [\mathbf{B}, \mathcal{B}^* = (\bar{b}_1, \bar{b}_2, \bar{b}_3)]$. The vectors $\bar{b}_2, \bar{b}_3$ necessarily lie on the cross-section of the beam but the vector $\bar{b}_1$ does not necessarily point in the unit tangential direction. The co-ordinates $\alpha_1, \alpha_2 and \alpha_3$ are used to represent the material co-ordinates of the beam, the last two co-ordinates represent the lengths in the $\bar{b}_2, \bar{b}_3$ directions respectively. It is preferable to work with non-dimensional co-ordinates in the three directions. It is preferrable to work with non-dimensional co-ordinates. For the remainder of this paper we assume that all length measurements have been normalized. The orientation of the sectional plane changes as it slides along the curve $\mathcal{C}$, making the basis $\mathcal{B}^*$ a function of the spanwise variable α_1. A rotation tensor $\underline{\underline{R}}(\alpha_1)$ brings the basis $\mathcal{I}$ to the basis $\mathcal{B}^*$. Subsequently the motion tensor $\underline{\underline{\mathcal{C}}}(\underline{\bar{r}}_B, \underline{\underline{R}})$ can be defined.

$$\underline{\underline{\mathcal{C}}}(\underline{\bar{r}}_B, \underline{\underline{R}}) = \begin{bmatrix} \underline{\underline{R}} & \tilde{\bar{r}}_B \underline{\underline{R}} \\ \underline{\underline{0}} & \underline{\underline{R}} \end{bmatrix} \tag{3.1}$$

The curvature tensor of the beam is defined as

$$\tilde{\bar{\mathcal{K}}}^* = \underline{\underline{\mathcal{C}}}^{-1} \underline{\underline{\mathcal{C}}}' \tag{3.2}$$

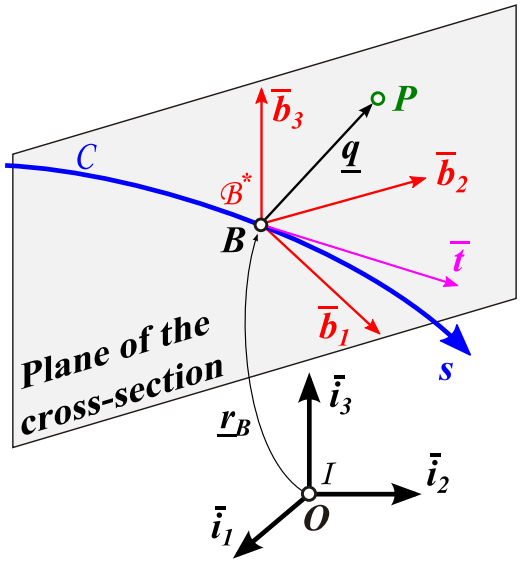

Fig. 3.1: Representation of a beam cross section.

Where $(')$ represents a derivative with respect to $\bar{\alpha}_1$ and $\underline{\bar{\mathcal{K}}}^{*T} = \{\bar{t}^{+T}, \underline{\bar{k}}^{*T}\}$, with $\underline{\bar{k}}^* = \text{axial}(\underline{\underline{R}}^T \underline{\underline{R}}')$ being the curvature vector. A detailed formulation of the above equations can be found in Bauchau [21].

3.1.1 Strain components

The formulation presented here is meant for large displacement and rotation problems however the strains are assumed to be small. We chose to work with the Green-Lagrange strain tensor partitioned into out-of-plane and in-plane strain components, $\underline{\gamma}_O^{*T} = \{\gamma_{11}^*, 2\gamma_{12}^*, 2\gamma_{13}^*\}$ and $\underline{\gamma}_I^{*T} = \{\gamma_{22}^*, \gamma_{33}^*, 2\gamma_{23}^*\}$, respectively, defined as

$$\sqrt{g}\ \underline{\gamma}_O^* = \underline{\bar{u}}^{*\prime} + \underline{\underline{\bar{D}}}_O \underline{\bar{u}}^* \tag{3.3a}$$

$$\sqrt{g}\ \underline{\gamma}_I^* = \quad \underline{\underline{\bar{D}}}_I\ \underline{\bar{u}}^* \tag{3.3b}$$

Where $\sqrt{g} = \bar{t}_1^* - \bar{k}_3^*\bar{\alpha}_2 + \bar{k}_2^*\bar{\alpha}_3$ and the following differential operators can be defined

$$\underline{\underline{\bar{D}}}_O = \begin{bmatrix} \bar{d} & -\bar{k}_3^* & \bar{k}_2^* \\ \bar{k}_3^* + \sqrt{g}\dfrac{\partial}{\partial\bar{\alpha}_2} & \bar{d} & -\bar{k}_1^* \\ -\bar{k}_2^* + \sqrt{g}\dfrac{\partial}{\partial\bar{\alpha}_3} & \bar{k}_1^* & \bar{d} \end{bmatrix} \tag{3.4}$$

$$\underline{\underline{\bar{D}}}_I = \begin{bmatrix} 0 & \sqrt{g}\dfrac{\partial}{\partial\bar{\alpha}_2} & 0 \\ 0 & 0 & \sqrt{g}\dfrac{\partial}{\partial\bar{\alpha}_3} \\ 0 & \sqrt{g}\dfrac{\partial}{\partial\alpha_3} & \sqrt{g}\dfrac{\partial}{\partial\bar{\alpha}_2} \end{bmatrix} \tag{3.5}$$

Where $\bar{d} = -(\bar{t}_2^* - \bar{k}_1^*\bar{\alpha}_3)\partial(\cdot)/\partial\bar{\alpha}_2 - (\bar{t}_3^* + \bar{k}_1^*\bar{\alpha}_2)\partial(\cdot)/\partial\bar{\alpha}_3$. Eq. (3.3) can be consolidated as

$$\underline{\gamma}^* = \begin{Bmatrix} \underline{\gamma}_O^* \\ \underline{\gamma}_I^* \end{Bmatrix} = \underline{\underline{\bar{A}}}\,\underline{\bar{u}}^{*\prime} + \underline{\underline{\bar{B}}}\,\underline{\bar{u}}^* \tag{3.6}$$

Where,

$$\underline{\underline{\bar{A}}} = \frac{1}{\sqrt{g}}\begin{bmatrix} \underline{\underline{I}} \\ \underline{\underline{0}} \end{bmatrix}, \quad \underline{\underline{\bar{B}}} = \frac{1}{\sqrt{g}}\begin{bmatrix} \underline{\underline{\bar{D}}}_O \\ \underline{\underline{\bar{D}}}_I \end{bmatrix} \tag{3.7}$$

3.2 Semi-discretization of the displacement field

Beam theory is essentially used to recast fully three-dimensional problems to a simpler one dimensional problem when standard underlying assumptions are

satisfied. We intend to do the same for our problem using a well known semi-discretization technique

$$\bar{\underline{u}}^*(\bar{\alpha}_1, \bar{\alpha}_2, \bar{\alpha}_3) = \bar{\underline{\underline{N}}}(\bar{\alpha}_2, \bar{\alpha}_3)\hat{\underline{u}}(\bar{\alpha}_1), \tag{3.8}$$

Using the technique prescribed in eq. (3.8) we can recast our problem such that the displacement field for the governing equations for the structural dynamics of the system be a function of the parameter $\bar{\alpha}_1$ exclusively. The matrix $\bar{\underline{\underline{N}}}(\bar{\alpha}_2, \bar{\alpha}_3)$ discretizes the cross section of the beam using two-dimensional shape functions used in the discretization whereas the vector $\hat{\underline{u}}(\bar{\alpha}_1)$ stores the nodal values of the displacement field. Once the displacement field $\hat{\underline{u}}(\bar{\alpha}_1)$ has been obtained we can recover cross sectional deformations and stresses using the formulations developed in the subsequent sections. As per standard nodal discretization for a problem containing N nodes the total number of degrees of freedom are $3N$. A graphical representation of the semi-discretization process can be seen in fig. 3.2.

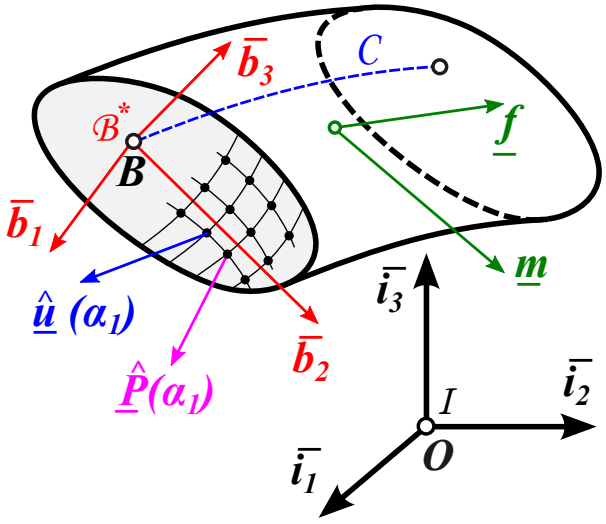

Fig. 3.2: Semi-discretization of the beam.

The given discretization yields the components of the Green-Lagrange strain tensor as

$$\underline{\gamma}^* = \underline{\underline{\bar{A}}}\,\underline{\underline{N}}\,\underline{\hat{u}}' + \underline{\underline{\bar{B}}}\,\underline{\underline{N}}\,\underline{\hat{u}} \tag{3.9}$$

For a rigid body motion the displacement field can be written as $\underline{u} = \underline{u}_R - \tilde{q}\underline{\phi}_R$ where $\underline{u}_R$ and $\underline{\phi}_R$ are components of rigid body translation and rotation respectively. For convenience the following non-dimensional motion array, $\underline{\bar{\mathcal{U}}}_R^T = \{\underline{\bar{u}}_R^T, \underline{\phi}_R^T\}$, can be identified and at a specific point of the cross section.

$$\begin{aligned}\begin{Bmatrix} \bar{u}_1^* \\ \bar{u}_2^* \\ \bar{u}_3^* \end{Bmatrix} = \underline{\bar{u}}_R^* - \tilde{\bar{q}}^*\underline{\phi}_R^* &= \begin{bmatrix} 1 & 0 & 0 & 0 & \bar{\alpha}_3 & -\bar{\alpha}_2 \\ 0 & 1 & 0 & -\bar{\alpha}_3 & 0 & 0 \\ 0 & 0 & 1 & \bar{\alpha}_2 & 0 & 0 \end{bmatrix} \begin{Bmatrix} \underline{\bar{u}}_R^* \\ \underline{\phi}_R^* \end{Bmatrix} \\ &= \underline{\underline{\bar{z}}}\,\underline{\bar{\mathcal{U}}}_R^* = \underline{\underline{N}}\,\underline{\underline{\bar{Z}}}\,\underline{\bar{\mathcal{U}}}_R^*\end{aligned} \tag{3.10}$$

Where $\underline{\bar{\mathcal{U}}}_R^* = \underline{\underline{\mathcal{C}}}^{-1}\underline{\bar{\mathcal{U}}}_R$ and matrix $\underline{\underline{\bar{Z}}}$ stacks the rows of matrix $\underline{\bar{z}}$ for each of the nodes of the model.

3.3 The central solution

The central solution is an exact solution of the linear theory of three dimensional elasticity for beams presenting uniform geometric and material characteristics along the span and is valid far away from the ends of the beam, where the effects due to the end conditions become negligible. The kinematic assumptions underpinning beam theories are eliminated and yet exact solutions for the central behavior

of the beam can be obtained. The only source of error is due to the discretization of problem using finite elements. The three-dimensional strains at any point can be recovered using the sectional forces and moments $\underline{\mathcal{F}}_c^{*T} = \{\underline{F}^{*T}, \underline{M}^{*T}\}$, evaluated at a given cross section, resolved in the basis $\mathcal{B}^*$. The three dimensional strain is recovered as

$$\underline{\gamma}_c^* = \begin{bmatrix} (\underline{\underline{\bar{A}}}\,\underline{\underline{N}}) & (\underline{\underline{\bar{B}}}\,\underline{\underline{N}}) \end{bmatrix} \underline{\underline{\bar{\mathcal{L}}}}_c^* \underline{\bar{\mathcal{F}}}_c^* = \underline{\underline{\bar{M}}}_c(\bar{\alpha}_2, \bar{\alpha}_3)\underline{\bar{\mathcal{F}}}_c^* \tag{3.11}$$

$$\underline{\underline{\bar{\mathcal{L}}}}_c^* = \begin{bmatrix} \underline{\underline{\bar{G}}}_c \\ \underline{\underline{\bar{W}}}_c \end{bmatrix} = \begin{bmatrix} \underline{\underline{\bar{Z}}}\,\underline{\underline{\bar{\mathcal{S}}}}_c^* + \underline{\underline{\bar{W}}}_c \tilde{\bar{\mathcal{K}}}^{*T} \\ \underline{\underline{\bar{W}}}_c \end{bmatrix} \tag{3.12}$$

$\underline{\bar{\mathcal{F}}}_c^*$ is an array of the non-dimensionalized sectional stress resultants and the notation $(\cdot)_c$ indicates quantities pertaining to the central solution. Matrix $\underline{\underline{\bar{W}}}_c$, of size $n \times 6$, stores the nodal warping field; the columns of this matrix represent the warping induced by unit sectional stress resultants. Matrix $\underline{\underline{\bar{G}}}_c$, of size $n \times 6$, stores the nodal displacements derivatives. Symmetric matrix $\underline{\underline{\bar{\mathcal{S}}}}_c^*$ is the sectional compliance matrix for the central solution, *i.e.*,

$$\underline{\bar{\mathcal{E}}}_c^* = \underline{\underline{\bar{\mathcal{S}}}}_c^* \underline{\bar{\mathcal{F}}}_c^* \tag{3.13}$$

Where array $\underline{\bar{\mathcal{E}}}_c^*$ stores the sectional strains consisting of the axial strain and two transverse shear strains, and the sectional curvatures consisting of the twist rate and two bending curvatures, all resolved in basis $\mathcal{B}^*$. Detailed derivations of the same can be found in Bauchau and Han [20, 22]. Thereafter, the components

of the Cauchy stress tensor can be evaluated using the material constitutive laws. Given a material stiffness tensor $\underline{\underline{\mathcal{D}}}^*_\infty$, of size 6×6, resolved the material basis.

$$\underline{\tau}^* = \underline{\underline{\mathcal{D}}}^*_\infty \underline{\gamma}^* \tag{3.14}$$

Chapter 4: Viscoelasticity for beams and joints

4.1 Viscoelastic theory for joints

As a precursor to the discussion on beams it is useful to go over the theory of viscoelastic joints and the solution techniques used to model their behavior. One dimensional rectilinear or torsional joints can be considered. More complicated joints such as flexible joints having all six degrees of freedom may also be considered. For a rectilinear/torsional joint the generalized Maxwell model can be designed simply as an arrangement of elastic springs and dashpots as shown in fig. 2.1. A stiffness value can be defined for the exclusively elastic branch and additional Maxwell fluid branches can be defined having elastic stiffnesses and a relaxation time. If a torsional damper is considered the total moment in the element is given as

$$M = k_\infty \theta + \sum_{n=1}^{N} k_n(\theta - \alpha_i) \tag{4.1}$$

As stated earlier quantities such as the storage modulus, the loss modulus and the phase difference can be evaluated as well. The solution for viscoelasticity can be generated by solving the evolution equation. The evolution equation for a Maxwell fluid branch of the torsional damper is given as

$$\tau_n \dot{\alpha_n} + \alpha_n = \theta \tag{4.2}$$

The subscript n is dropped in the subsequent formulation for the sake of simplicity. The evolution equation can be recast in terms of a non-dimensional time quantity, η. Over a given time step, $[t : t_i \leq t \leq t_f]$ the quantity η is given as $\eta = (t - t_i)/h$ where $h = t_f - t_i$ and subscripts, $(.)_i$ and $(.)_f$ represent the state at the initial and final time of the time step. This changes our equation to the form $\alpha' + \bar{h}\alpha = \bar{h}\theta(\eta)$, where $(.)'$ is a derivative with respect to η, $\bar{h} = h/\tau$. For a small enough time step we can assume a linear evolution of the angular displacement θ. This gives us $\theta(\eta) = \theta_i + \eta(\theta_f - \theta_i)$. Multiplying the equation in terms of η with $e^{\bar{h}\eta}$, it can be recast as

$$[\alpha e^{\bar{h}\eta}]' = \bar{h} e^{\bar{h}\eta}[\theta_i + \eta(\theta_f - \theta_i)] \tag{4.3}$$

Integrating the equation form time t_i to t_f gives us

$$\alpha_f - \theta_f = (\alpha_i - \theta_i)\Gamma_1 - (\theta_f - \theta_i)\Gamma_2 \tag{4.4}$$

Where the parameters Γ_1 and Γ_2 are defined as

$$\Gamma_1 = e^{-\bar{h}}, \Gamma_2 = \frac{1 - e^{-\bar{h}}}{\bar{h}} \tag{4.5}$$

4.2 Flexible joint

A simple flexible joint can be represented as shown in fig. 4.1. The two ends of the joint are denoted K and L. To evaluate the effect on a system due to a flexible joint we will need to evaluate the relative motion between the two end. A complete formulation for a flexible joint from a flexible joint is presented in Bauchau and Han [23]. If we consider the two handles as represented in the figure the main quantity that is required to be known is the relative motion between the two joints. The relative motion can be defined as

$$\underline{\underline{\mathcal{S}}} = (\underline{\underline{\mathcal{C}}}_k^* \underline{\underline{\mathcal{R}}}_0^*)^{-1} (\underline{\underline{\mathcal{C}}}_l^* \underline{\underline{\mathcal{R}}}_0^*) \tag{4.6}$$

The forces acting on the two handles resolved in the material frames are given as $\underline{\mathcal{A}}_k$ and $\underline{\mathcal{A}}_l$ respectively.

$$\underline{\underline{\mathcal{S}}}^T \underline{\mathcal{A}}_k + \underline{\mathcal{A}}_l = 0 \tag{4.7}$$

The differential work done by the applied loading is given as

$$dW = \underline{\mathcal{A}}_k^T (\underline{\underline{\mathcal{R}}}_0^{*-1} \underline{\mathrm{d}\mathcal{U}}_k) + \underline{\mathcal{A}}_l^T (\underline{\underline{\mathcal{R}}}_0^{*-1} \underline{\mathrm{d}\mathcal{U}}_l) = \underline{\mathcal{A}}_l^T [\underline{\underline{\mathcal{R}}}_0^{*-1} \underline{\mathrm{d}\mathcal{U}}_l - (\underline{\underline{\mathcal{R}}}_0 \underline{\underline{\mathcal{S}}})^{*-1} \underline{\mathrm{d}\mathcal{U}}_k] = \underline{\mathcal{A}}^T \underline{\mathrm{d}\mathcal{U}}_r \tag{4.8}$$

Where $\underline{\mathrm{d}\mathcal{U}}_k$, $\underline{\mathrm{d}\mathcal{U}}_l$ and $\underline{\mathrm{d}\mathcal{U}}_r$ are the displacements of the two handles separately and the relative displacement between them in the material frame respectively. We

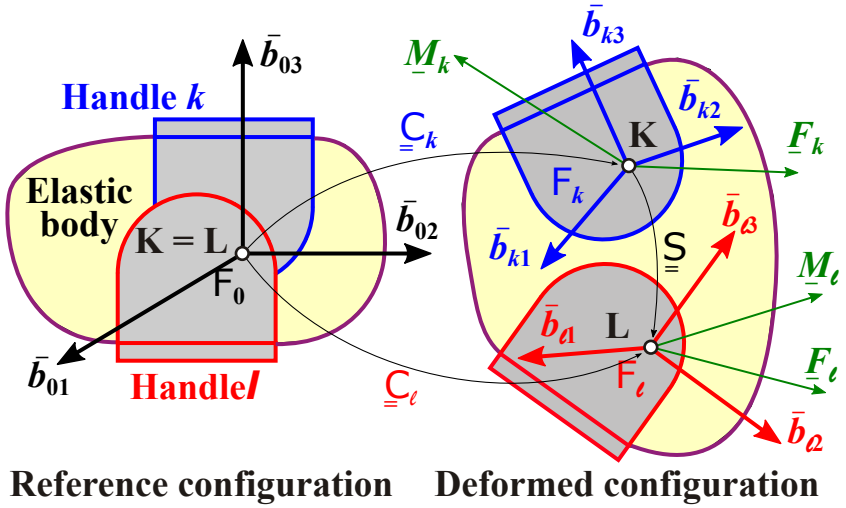

Fig. 4.1: Representation of a flexible joint.

also consider $\underline{\mathcal{A}}_l = \underline{\mathcal{A}}$ since the two forces are essentially equal and opposite when resolved in the same frame of reference. We now look to model the formulation within a multibody dynamics framework. The differential work can be rewritten as

$$dW = \underline{\mathcal{A}}^T \underline{\underline{\mathcal{T}}}(-\underline{\mathcal{E}})\mathrm{d}\underline{\mathcal{E}} = \underline{\mathcal{F}}^T \mathrm{d}\underline{\mathcal{E}} \tag{4.9}$$

Where $\underline{\underline{\mathcal{T}}}$ is the required tangent tensor and $\underline{\mathcal{E}}$ the parameterized measure of deformation given by the relation $\underline{\mathrm{d}\mathcal{U}_r} = \underline{\underline{\mathcal{T}}}(-\underline{\mathcal{E}})\underline{\mathrm{d}\mathcal{E}}$. Hence, the generalized forces associated with the generalized deformation measure $\underline{\mathcal{E}}$, $\underline{\mathcal{F}}$ are given as

$$\begin{aligned} \underline{\mathcal{F}}^T &= \underline{\mathcal{A}}^T \underline{\underline{\mathcal{T}}}(-\underline{\mathcal{E}}), \\ \underline{\mathcal{E}} &= \begin{Bmatrix} \underline{\epsilon} \\ \underline{\kappa} \end{Bmatrix} \end{aligned} \tag{4.10}$$

Where $\underline{\epsilon}$ and $\underline{\kappa}$ give us the required strains and curvatures respectively. If we

assume that the flexible joint is made of an elastic material th generalized forces can be derived from a potential function, A. Hence we have

$$\underline{\mathcal{F}} = \frac{\partial A(\underline{\mathcal{E}})}{\partial \underline{\mathcal{E}}} \tag{4.11}$$

Naturally the variation of the potential function, equivalent to a strain energy function, can be represented in the variational for as follows

$$\delta A = \delta \underline{\mathcal{E}}^T \underline{\underline{\mathcal{K}}}^e \underline{\mathcal{E}} = \delta \underline{\mathcal{E}}^T \underline{\mathcal{F}}^e \tag{4.12}$$

$\underline{\underline{\mathcal{K}}}^e$ represents the flexible joint's elastic stiffness matrices and $\underline{\mathcal{F}}^e$ the elastic forces. The deformation measure $\underline{\mathcal{E}}$ and the relative displacement vector can be related as follows

$$\delta \underline{\mathcal{E}} = \underline{\underline{\mathcal{T}}}^{-1}(-\underline{\mathcal{E}}) \delta \underline{\mathcal{U}}_r = \underline{\underline{\mathcal{T}}}^{-1}(-\underline{\mathcal{E}}) \underline{\underline{G}}(\underline{\mathcal{E}}) \underline{\underline{R}}_0^{-1} \delta \underline{\mathcal{U}} = \underline{\underline{B}}\, \delta \underline{\mathcal{U}} \tag{4.13}$$

Where

$$\underline{\underline{G}} = \begin{bmatrix} -\underline{\underline{\mathcal{S}}}^{-1} & \underline{\underline{\mathcal{I}}} \end{bmatrix}$$

$$\underline{\underline{R}}_0 = \begin{bmatrix} \underline{\underline{\mathcal{R}}}^*_{k0} & \underline{\underline{0}} \\ \underline{\underline{0}} & \underline{\underline{\mathcal{R}}}^*_{l0} \end{bmatrix}$$

$$\underline{\delta\mathcal{U}} = \begin{Bmatrix} \underline{\delta\mathcal{U}}_k \\ \underline{\delta\mathcal{U}}_l \end{Bmatrix}$$

$$\underline{\underline{B}} = \left[-\underline{\underline{\mathcal{T}}}^{-1}(\underline{\mathcal{E}}) \quad \underline{\underline{\mathcal{T}}}^{-1}(-\underline{\mathcal{E}}) \right] \underline{\underline{R}}_0^{-1}$$

The tangent tensor $\underline{\underline{\mathcal{T}}}^{-1}(\underline{\mathcal{E}})$ is given as

$$\underline{\underline{\mathcal{T}}}^{-1}(\underline{\mathcal{E}}) = \boldsymbol{\chi}_0 \underline{\underline{I}} - \frac{1}{2}\tilde{\mathcal{E}} + \boldsymbol{\chi}_2 \tilde{\mathcal{E}}\tilde{\mathcal{E}} \tag{4.14}$$

With parameters $\boldsymbol{\chi}_0$ and $\boldsymbol{\chi}_2$ given as

$$\begin{aligned} \boldsymbol{\chi}_0 &= \mathcal{E}' \\ \boldsymbol{\chi}_2 &= \frac{1}{\mathcal{E}^2}(\mathcal{E}' - \frac{1}{\boldsymbol{\varepsilon}}) \\ \boldsymbol{\varepsilon} &= \frac{2tan(\phi/2)}{\mathcal{E}} \end{aligned} \tag{4.15}$$

The generalized elastic forces in the flexible joint can now be written as

$$\underline{F}^e = \underline{\underline{B}}^T \underline{\mathcal{F}}^e \tag{4.16}$$

Eq. (4.16) can finally now be linearized to obtain the equations that would need to be solved in order to solve the dynamic simulation.

$$\Delta\underline{F}^e = \underline{\underline{K}}^e \underline{\Delta\mathcal{U}} \tag{4.17}$$

The stiffness matrix written in terms of the strain interpolation matrix, $\underline{\underline{B}}$ and the tangent tensor, $\underline{\underline{H}}$ is given as

$$\underline{\underline{K}}^e = \underline{\underline{B}}^T(\underline{\mathcal{E}})\underline{\underline{\mathcal{K}}}^e\underline{\underline{B}}(\underline{\mathcal{E}}) + \underline{\underline{H}}^T(\underline{\mathcal{F}}^e)\underline{\underline{B}}(\underline{\mathcal{E}}) \tag{4.18}$$

Where $\underline{\underline{H}}$ is a tangent tensor given as

$$\underline{\underline{H}}(\underline{\mathcal{F}}^e) = \begin{bmatrix} -\underline{\underline{\mathcal{L}}}^{\flat T}(\underline{\mathcal{E}}, \underline{\mathcal{F}}^e) & \underline{\underline{\mathcal{L}}}^{\flat T}(-\underline{\mathcal{E}}, \underline{\mathcal{F}}^e) \end{bmatrix} \underline{\underline{R}}_0^{-1} \tag{4.19}$$

Where the operator $\underline{\underline{\mathcal{L}}}^{\flat T}(\underline{\mathcal{E}}, \underline{\mathcal{F}}^e)$ is given as

$$\underline{\underline{\mathcal{L}}}^{\flat}(\underline{\mathcal{E}}, \underline{\mathcal{F}}) = (\hat{\boldsymbol{\chi}}_0 + \hat{\boldsymbol{\chi}}_2\tilde{\mathcal{E}}\tilde{\mathcal{E}})^T\underline{\underline{P}}^{\flat} - \frac{1}{2}\tilde{\mathcal{F}}^{\flat} + 2(\boldsymbol{\chi}_2\tilde{\mathcal{E}})^T\tilde{\mathcal{F}}^{\flat} + \tilde{\mathcal{F}}^{\flat}(\boldsymbol{\chi}_2\tilde{\mathcal{E}}) \tag{4.20}$$

Where $\underline{\underline{P}}^{\flat}$ is given as

$$\underline{\underline{P}}^{\flat} = \begin{bmatrix} \underline{\underline{0}} & \underline{f}^o\underline{e}^T \\ \underline{f}^o\underline{e}^T & \underline{f}\underline{e}^T + \underline{f}^o\underline{e}^{oT} \end{bmatrix} \tag{4.21}$$

The formulation discussed in the previous section can be modified to work for problems involving viscoelasticity in flexible joints. The generalized Maxwell model for the flexible joint can be shown as in fig. 4.2.

The internal state parameters for each viscoelastic branch, b are given as $\underline{\mathcal{S}}^b$. The force in each viscoelastic branch is then given as $\underline{\mathcal{F}}^b = \underline{\underline{\mathcal{K}}}^b(\underline{\mathcal{E}} - \underline{\mathcal{S}}^b)$, where $\underline{\underline{\mathcal{K}}}^b$ gives us the stiffness matrix of the elastic elements in every Maxwell fluid branch.

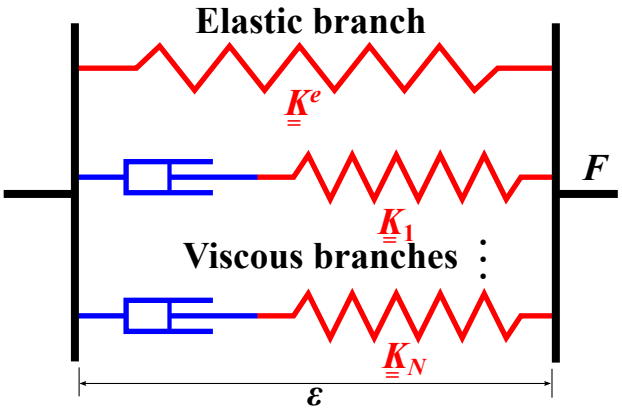

Fig. 4.2: Generalized Maxwell model for a flexible joint.

An additional parameter τ^b is also defined for each branch, which relates the internal state parameters with the deformation measure for each branch as follows

$$\tau^b \dot{\underline{\mathcal{S}}}^b + \underline{\mathcal{S}}^b = \underline{\mathcal{E}} \tag{4.22}$$

The given evolution equation can be solved as was done in the previous section. If the forces in the Maxwell fluid can be given as

$$\underline{\mathcal{F}}_f^b = \Gamma_1^b \underline{\mathcal{F}}_i^b + \Gamma_2^b \underline{\underline{\mathcal{K}}}^b (\underline{\mathcal{E}}_f - \underline{\mathcal{E}}_i) \tag{4.23}$$

Where the subscripts i and f represent the initial and final states over a given time step. The total force acting on the flexible joint is given as $\underline{\mathcal{F}}_f^t = \underline{\mathcal{F}}_f^e + \sum_{b=1}^{N} \underline{\mathcal{F}}_f^b$. The total stiffness is given as a sum of the stiffnesses arising out of the Maxwell fluid branches.

$$\Delta \underline{F}_f^b = \underline{\underline{K}}^b \Delta \underline{\mathcal{U}}_f$$

$$\underline{\underline{K}}^b = \underline{\underline{B}}^T(\underline{\mathcal{E}}_f) \Gamma_2^b \underline{\underline{\mathcal{K}}}^b \underline{\underline{B}}(\underline{\mathcal{E}}_f) + \underline{\underline{H}}^T(\underline{\mathcal{F}}_f^b) \underline{\underline{B}}(\underline{\mathcal{E}}_f) \tag{4.24}$$

$$\underline{\underline{K}}^t = \underline{\underline{B}}^T(\underline{\mathcal{E}}_f)\underline{\underline{\mathcal{K}}}^t\underline{\underline{B}}(\underline{\mathcal{E}}_f) + \underline{\underline{H}}^T(\underline{\mathcal{F}}_f^t)\underline{\underline{B}}(\underline{\mathcal{E}}_f) \tag{4.25}$$

and

$$\underline{\underline{\mathcal{K}}}^t = \underline{\underline{\mathcal{K}}}^e + \sum_{b=1}^{N} \Gamma_2^b \underline{\underline{\mathcal{K}}}^b$$

4.3 Viscoelastic beam theory

In this section viscoelastic formulations that can be used alongside the 3-D beam theory discussed in the previous chapter are presented. We notice that the general structure of the viscoelastic relations are similar to those obtained for joints. For viscoelastic beams the sectional stress resultants, $\underline{\mathcal{F}}^*$ can be expressed as

$$\underline{\mathcal{F}}^* = \int_{\mathcal{A}} \underline{\underline{z}}^T \underline{\tau}_o^* d\mathcal{A} = \int_{\mathcal{A}} \begin{bmatrix} \underline{\underline{z}}^T & \underline{\underline{0}} \end{bmatrix} \underline{\tau}^* d\mathcal{A} \tag{4.26}$$

Where $\underline{\underline{z}}$ was described earlier and $\underline{\tau}_o^*$ and $\underline{\tau}^*$ represent the out-of-plane and the combined in-plane and out-of-plane stresses in the cross section respectively. Introducing the convolution form of the generalized Maxwell model we have

$$\underline{\mathcal{F}}^* = \int_{\mathcal{A}} \begin{bmatrix} \underline{\underline{z}}^T & \underline{\underline{0}} \end{bmatrix} \left[\int_{-\infty}^{t} \underline{\underline{G}}^*(t-s)\dot{\underline{\gamma}}^*(s) ds \right] d\mathcal{A} \tag{4.27}$$

Using the relationship given in eq. (3.11) we can express the sectional stresses in terms of the recovery relationships as we had done for regular problems without viscoelasticity. We have

$$\begin{aligned}\underline{\mathcal{F}}^* &= \int_{-\infty}^{t}\left[\int_{\mathcal{A}}\begin{bmatrix}\underline{\underline{z}}^T & \underline{\underline{0}}\end{bmatrix}\underline{\underline{G}}^*(t-s)\underline{\underline{M}}_c^* d\mathcal{A}\right]\dot{\underline{\mathcal{F}}}_c^* ds \\ &= \int_{-\infty}^{t}\underline{\underline{\mathcal{H}}}^*(t-s)\dot{\underline{\mathcal{E}}}_c^* ds\end{aligned} \tag{4.28}$$

Where $\underline{\mathcal{E}}_c^*$ are the sectional strains in the system and for a generalized Maxwell Viscoelastic material with N branches, $\underline{\underline{\mathcal{H}}}^*$ is a sectional relaxation function given as

$$\begin{aligned}\underline{\underline{\mathcal{H}}}^* &= \underline{\underline{\mathcal{C}}}_\infty^* + \sum_{b=1}^{N}\underline{\underline{\mathcal{C}}}_b^* \exp^{-t/\tau_b} \\ \underline{\underline{\mathcal{C}}}_\infty^* &= [\int_{\mathcal{A}}\begin{bmatrix}\underline{\underline{z}}^T & \underline{\underline{0}}\end{bmatrix}\underline{\underline{D}}_\infty^*\underline{\underline{M}}_c^* d\mathcal{A}]\underline{\underline{C}}_c^* \\ \underline{\underline{\mathcal{C}}}_b^* &= [\int_{\mathcal{A}}\begin{bmatrix}\underline{\underline{z}}^T & \underline{\underline{0}}\end{bmatrix}\underline{\underline{D}}_b^*\underline{\underline{M}}_c^* d\mathcal{A}]\underline{\underline{C}}_c^*\end{aligned} \tag{4.29}$$

Where $\underline{\underline{\mathcal{C}}}_c^*$ is the sectional stiffness matrix as derived in earlier sections. If we assign six internal states, $\underline{\mathcal{J}}_b$ corresponding to the six sectional deformations for each Maxwell fluid branch we can prescribe an evolution equation for a Maxwell fuid branch of the form

$$\tau_b\dot{\underline{\mathcal{J}}}_b + \underline{\mathcal{J}}_b = \underline{\mathcal{E}}_c^* \tag{4.30}$$

The evolution equations can be solved as we had done earlier

$$\begin{aligned}\underline{\mathcal{F}}_t &= \underline{\mathcal{F}}_\infty + \sum_{N_b=1}^{N_b}\underline{\mathcal{F}}_b \\ \underline{\mathcal{F}}_f^{*b} &= \Gamma_1^b\underline{\mathcal{F}}_i^{*b} + \Gamma_2^b\underline{\underline{C}}_b^*(\underline{\mathcal{E}}_{cf}^* - \underline{\mathcal{E}}_{ci}^*)\end{aligned} \tag{4.31}$$

4.3.1 *Prediction of stresses*

Having done a one- dimensional beam analysis we will be interested to predict accurately, the stresses appearing on any given location on the beam. This can be done easily using the recovery relationships we have developed earlier. They can be used to obtain exact values of three dimensional stresses at any given location. Thereafter the evolution equation of the stresses can be solved to obtain the three dimensional stresses. Assuming we ave six internal states, $\underline{\nu}_b$ associated with the three dimensional strains for every Maxwell fluid branch we have

$$\tau^b \underline{\dot{\nu}}^b + \underline{\nu}^b = \underline{\gamma}^*_c \tag{4.32}$$

The stresses can be obtained by solving the above equation. The stresses can be easily obtained in terms of the sectional stress resultants for the elastic branch as follows

$$\begin{aligned} \underline{\underline{D}}^*_b(\underline{\gamma}^*_{cf} - \underline{\nu}^{b*}_f) &= \Gamma^b_1 \underline{\underline{D}}^*_b(\underline{\gamma}^*_{ci} - \underline{\nu}^{b*}_i) + \Gamma^b_2 \underline{\underline{D}}^*_b(\underline{\gamma}^*_{cf} - \underline{\gamma}^*_{ci}) \\ \underline{\sigma}^b_f &= \Gamma^b_1 \underline{\sigma}^b_i + \Gamma^b_2 \underline{\underline{D}}^*_b \underline{\underline{M}}^*_c (\underline{\mathcal{F}}^*_f - \underline{\mathcal{F}}^*_i) \end{aligned} \tag{4.33}$$

4.3.2 *Important assumptions*

There are some important assumptions that have to be kept in mind while using the above formulation. The problem we are looking to solve must be (1) a low frequency problem and (2) the structure must be lightly damped. Fundamentally beam theory is a "low-frequency approximation" for a fully three dimensional problem. The same was concluded by Volovoi et al. [24] and Han and Bauchau [25].

An important assumption associated with beam-theory is that the kinetic energy associated with the warping field is low. However for a high-frequency dynamical problem the effects manifest in the form of vibrations at characteristic length scales smaller or comparable to the cross sectional dimensions. This will lead to significant warping effects which will have to be considered separately. Secondly, the forces associated with damping for our problem have to be small. This is important for predicting the resulting viscous stresses correctly, using the elastic counterparts as shown previously. These assumptions do not impose any additional restrictions on our ability to solve a given problem because beam theory in the absence of viscoelasticity is inherently a low frequency problem. The low-frequency assumption can be cast in mathematical terms using the strain recovery relationships as follows

$$\underline{\dot{\gamma}}_c^* = \underline{\underline{M}}_c^* \underline{\dot{\mathcal{F}}}_c^* \tag{4.34}$$

Chapter 5: Numerical Examples

5.1 Torsional viscoelastic damper

5.1.1 Mathematical formulation

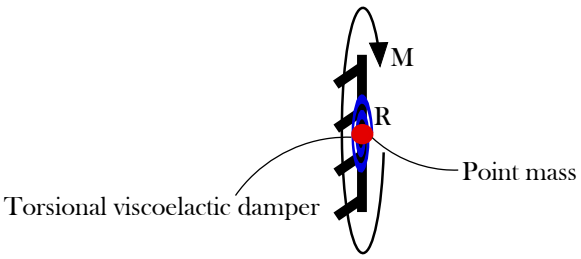

Fig. 5.1: 1-dimensional problem modeled using Dymore.

As an initial example problem we consider a one-dimensional torsional viscoelastic damper is connected to a point mass at point R as shown in fig. 5.1 A Zener element is used to model the damper. The damper has the following parameters, stiffness of the elastic branch, $k_\infty = 1000N - m/rad$ whereas the Maxwell fluid branch has a stiffness $k_1 = 400N - m/rad$ and relaxation time $\tau_1 = 0.1s$. Subsequently, an element having two additional Maxwell fluid branches with parameters, $k_2 = 200N - m/rad$, $\tau_2 = 0.05s$ and $k_3 = 300N - m/rad$, $\tau_3 = 0.075s$ is considered as well. A sinusoidally varying moment, M was applied at the fixed end R having an amplitude $40N - m$ and a varying frequency. The natural frequencies that were selected for the excitation function were 0.5, 0.75, 1, 2.5, 5, 7.5, 10, 25, 50, 75, 100,

250, 500 rad/sec. Analytical expressions presented earlier can be used to evaluate the storage modulus, the loss modulus, the rotation amplitude and the phase difference. The analytical solutions of the loss and storage modulus for the problem can be given as

$$G_s(\omega) = k_\infty + \sum_{n=1}^{N} k_n \frac{(\omega\tau_n)^2}{1 + (\omega\tau_n)^2} \tag{5.1}$$

$$G_l(\omega) = \sum_{n=1}^{N} k_n \frac{\omega\tau_n}{1 + (\omega\tau_n)^2} \tag{5.2}$$

$$|G(\omega)| = \sqrt{G_l(\omega)^2 + G_s(\omega)^2} \tag{5.3}$$

An analytical solution for the rotation amplitude $\theta(\omega_i)_{max}$ and the phase difference, $\phi(\omega_i)$ at the joint for a given frequency ω can be obtained as

$$\theta(\omega)_{max} = \frac{M_{max}}{\sqrt{G_l(\omega)^2 + G_s(\omega)^2}} \tag{5.4}$$

$$\phi(\omega) = tan^{-1}(\frac{G_l(\omega)}{G_s(\omega)}) \tag{5.5}$$

To get numerical solutions, this solution for the amplitude can be used to get a reference energy level which can be used as a convergence criterion. An approximate reference energy level, E_{ref} for a given ω for our problem can be given as

$$E_{ref} = \frac{1}{2}(k_1 + k_2)(\theta(\omega)_{max})^2 \tag{5.6}$$

So for $\omega = 50\ rad/sec$, $E_{ref} = .5 * (1400) * (0.0286)^2 \approx 0.57Nm$. Dynamic analysis was done for the selected excitation frequencies. Once a harmonic solution is obtained for the rotation in the damper, the displacement profile is extracted for one cycle of the time period. The amplitude of the response over this time period gives us the response amplitude, ($\theta^{Dymore}_{amplitude}$). The phase difference is evaluated as the inverse sine of the ratio of the first observed response in the extracted response cycle (θ^{Dymore}_{nT+h}), where nT is the elapsed time after n excitation cycles and h the time step size being used by the iterative solver.

$$\phi = sin^{-1}(\frac{\theta_{nT+h}}{\theta_{max}}) \tag{5.7}$$

From which we get

$$G(\omega) = \frac{M_{max}}{\theta_{max}} \tag{5.8}$$

$$G_l(\omega) = G(\omega)sin(\phi) \tag{5.9}$$

$$G_s(\omega) = G(\omega)cos(\phi) \tag{5.10}$$

The analytically obtained results were compared with the results obtained

using Dymore. They are presented in fig. 5.2 Additionally other quantities, like the stroke rates in the viscous dampers, $\dot{\alpha}$, the dissipative force, F^d, the viscous power, P^d and the energy dissipation, E^d can be obtained analytically as well. Whe have

$$\dot{\alpha_{b_i}} = \frac{1}{\tau_b}(\theta_i - \alpha_{b_i}) \tag{5.11}$$

$$F^d_{b_i} = k_b \tau_b (\theta_i - \alpha_{b_i}) \tag{5.12}$$

$$P^d_{b_i} = F^d_{b_i} \dot{\alpha_{b_i}} \tag{5.13}$$

$$E^d_{b_i} = \frac{1}{2}(P^d_{b_i} + P^d_{b_{i-1}})h \tag{5.14}$$

Where a subscript b is an index for a given Maxwell fluid branch of the elastomeric damper. The results obtained for the given quantities is

5.1.2 Discussion

- The number of cycles for which the dynamic analysis needs to be run has to be carefully selected. Depending on the value of the relaxation time, τ we have selected, the time it takes for our solution to become periodic will vary. In order to be sure about weather the solution had indeed become periodic we can take the help of the parameter α. If we observe the evolution of the parameter, α we find that it attains periodicity only after a certain

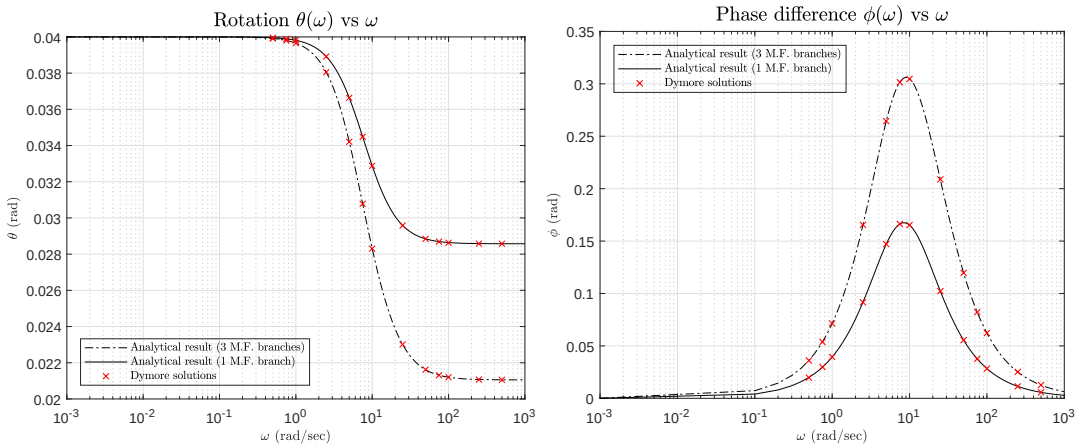

(a) Maximum observed rotation amplitude

(b) Phase difference

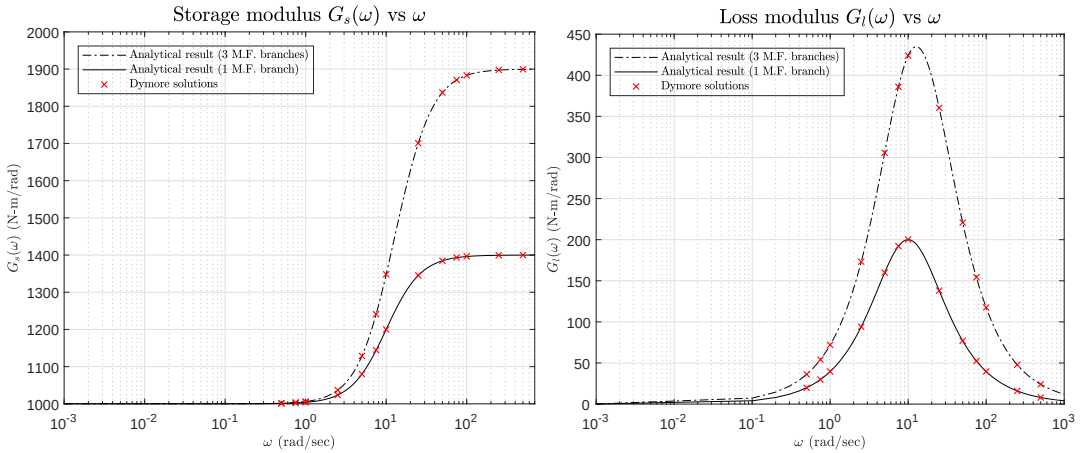

(c) Storage modulus

(d) Loss modulus

Fig. 5.2: Excitation frequency based variations in viscoelastic model properties.

number of excitation cycles. The number of cycles it takes for α to become periodic depends on the excitation frequency. Intuitively, we know that the parameter τ can be looked at as a characteristic time that tells us how long it would take for a viscoelastic element to regain its original shape after it has been deformed. For a harmonically applied loading, depending on time period of the excitation, the actual time it takes for the viscoelastic element to begin to behave periodically may vary because of the interplay between the viscoelastic element trying to relax and the harmonic excitation working

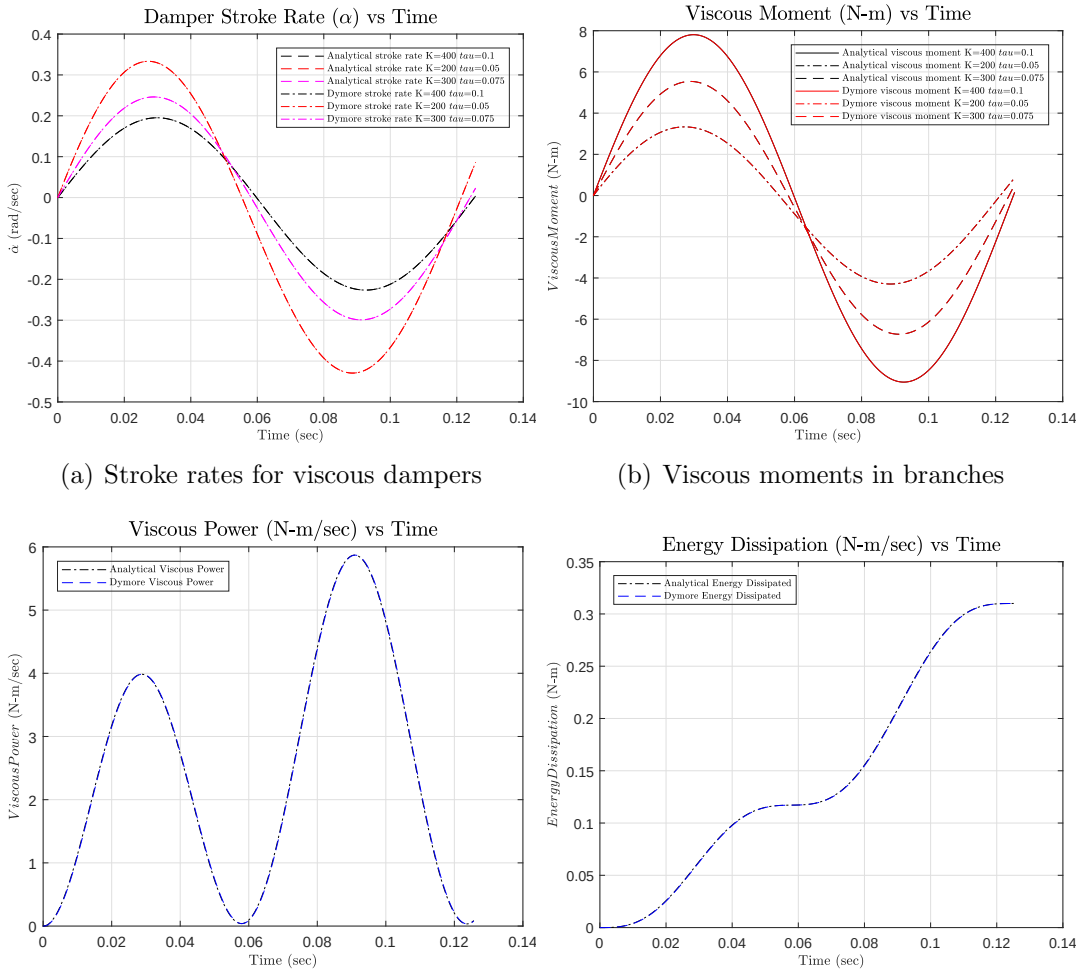

(a) Stroke rates for viscous dampers

(b) Viscous moments in branches

(c) Viscous power

(d) Energy dissipation

Fig. 5.3: Validation of quantities for an elastomeric damper element with a analytical results.

to further deform the element. Clearly, the interaction of these two effects is much more pronounced for high frequency excitations. This is exactly what we find for high excitation frequencies like 250 rad/sec. While 10 excitation cycles might be enough to attain periodicity in the case of lower excitation frequencies, 50 cycles are needed for an excitation frequency of 250 rad/sec. The response of the parameter α and associated quantities like $\dot{\alpha}$ and the dissipative moment generated M^d for an excitation of 250 rad/sec are plotted

in the results section.

- An exact comparison was also found for the evolution equation with respect top the discretized solution worked out earlier. To get an exact solution we can use the ODE45 solver in MATLAB. Assuming linear evolution of the overall strain over a small time step we can set up the evolution equation over a time step $t \in [t_i, t_f]$ as

$$\tau_n \dot{\alpha}_n + \alpha_n = \epsilon_i + \frac{t - t_i}{t_f - t_i}(\epsilon_f - \epsilon_i) \tag{5.15}$$

  A comparison of the exact solution obtained using the ODE45 solver and the discretized solution obtained in the previous sections is also compared in the results.

5.2 Flexible joint

5.2.1 Mathematical formulation

The flexible joint provides us the possibility of introducing displacements in all six degrees of freedom. As the simplest case, a flexible joint can be modeled as a set of six decoupled springs, acting along each of the six degrees of freedom, which presents us with a diagonal stiffness matrix. The complexity of the structural model of the joint can be progressively increased. For starters flexible joint can be assumed to be made out of an isotropic material which would simply provide us with coupling amongst the direct stresses and fully decoupled shear stresses. Anisotropy

can be progressively added to the material until we have a fully anisotropic stiffness matrix for the most general cases.

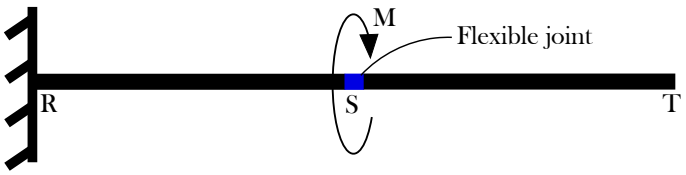

Fig. 5.4: Flexible joint problem modeled in Dymore.

As a validation problem, two beams RS and ST joined at point S with the help of a flexible joint were considered as shown in fig. 5.4. Within Dymore, viscoelasticity can be introduced in a flexible joint by addition of Maxwell fluid branches. A torsional moment M equal to $40N - m$ was applied on the vertex S of the beam ST, as was done in the earlier problem. In order to validate the flexible joint model with the one dimensional spring problem we chose to set up the stiffness matrix of the flexible joint element as a diagonal matrix. All the elements of the stiffness matrix except for the torsional degree of freedom are set to high values in order to effectively constrain those degrees of freedom. The elastic stiffness of the flexible joint in the torsional degree of freedom is set to $k_1 = 1000N - m/rad$ and that of the Maxwell fluid branches set to $k_2 = 400N - m/rad$, $k_3 = 200N - m/rad$ and $k_4 = 300N - m/rad$ with a relaxation times of $\tau_2 = 0.1s$, $\tau_3 = 0.05s$ and $\tau_4 = 0.075s$. The stiffness matrix of the flexible joint is defined as

$$\underline{\underline{\mathcal{K}}}^t = \underline{\underline{\mathcal{K}}}^e + \sum_{b=1}^{N_b} \Gamma_2^b \underline{\underline{\mathcal{K}}}^b \tag{5.16}$$

Where $\underline{\underline{\mathcal{K}}}^t$ is the matrix of the total stiffness of the flexible joint, $\underline{\underline{\mathcal{K}}}^e$ is the stiffness matrix of the elastic branch and $\underline{\underline{\mathcal{K}}}^b$ is the stiffness matrix for each of the

viscoelastic branches of the flexible joint.

The total force in the flexible joint is given as

$$\underline{\mathcal{F}}^t = \underline{\mathcal{F}}^e + \sum_{b=1}^{N_b} \underline{\mathcal{F}}^b \tag{5.17}$$

$$\underline{\mathcal{F}}^b = \underline{\underline{\mathcal{K}}}^b(\underline{\mathcal{E}} - \underline{\mathcal{A}}^b) \tag{5.18}$$

Where $\underline{\mathcal{F}^t}$, $\underline{\mathcal{F}^e}$ and $\underline{\mathcal{F}^b}$ represent the forces in the flexible joint, the elastic branch and the Maxwell fluid branches respectively. $\underline{\mathcal{E}}$ is used to represent the total displacement of the flexible joint and $\underline{\mathcal{A}^b}$ the displacement of the viscous element in a Maxwell fluid branch. As was done for the elastomeric damper an evolution equation can be prescribed for Maxwell fluid branches in the flexible joint.

$$\tau^b \underline{\dot{\mathcal{A}}}^b + \underline{\mathcal{A}}^b = \underline{\mathcal{E}} \tag{5.19}$$

τ^b is the relaxation time for a given Maxwell fluid branch. The evolution equation can also be integrated in a similar manner which gives us

$$\underline{\mathcal{A}}_f^b - \underline{\mathcal{E}}_f = {\Gamma_1}^b(\underline{\mathcal{A}}_i^b - \underline{\mathcal{E}}_i) - {\Gamma_2}^b(\underline{\mathcal{E}}_f - \underline{\mathcal{E}}_i) \tag{5.20}$$

We use the results obtained for the elastomeric damper with three Maxwell fluid branches in the previous to validate the results for the flexible joint. The stroke of the flexible joint was compared to that obtained for the elastomeric damper and we find that they match exactly as do other quantities such as the stroke rates in

the viscous elements of the Maxwell fluid branches, $\underline{\dot{\mathcal{A}}}$, the viscous forces in the branches, $\underline{\mathcal{F}}_d$, the total viscous power, P^d and the total energy dissipation, E^d. They are obtained as

$$\underline{\dot{\mathcal{A}}}_i^b = \frac{1}{\tau^b}(\underline{\mathcal{E}}_i - \underline{\mathcal{A}}_i^b) \tag{5.21}$$

$$\underline{\mathcal{F}}_i^b = \underline{\underline{\mathcal{K}}}^b(\underline{\mathcal{E}}_i - \underline{\mathcal{A}}_i^b) \tag{5.22}$$

$$P_{d_i}^b = \underline{\mathcal{F}}_i^{bT}\underline{\dot{\mathcal{A}}}_i^b \tag{5.23}$$

$$E_{d_i}^b = \frac{1}{2}(P_{d_i}^b + P_{d_{i-1}}^b)h \tag{5.24}$$

The results can be found in fig. 7 and 8.

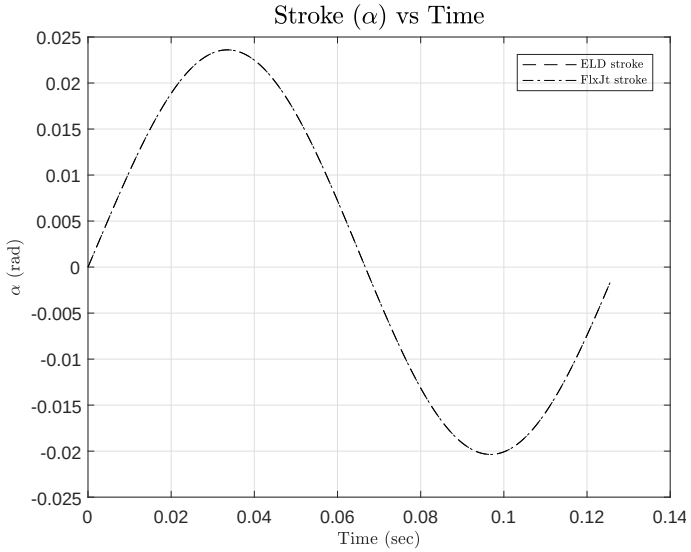

Fig. 5.5: Rotation in elastomeric bearing and flexible joint.

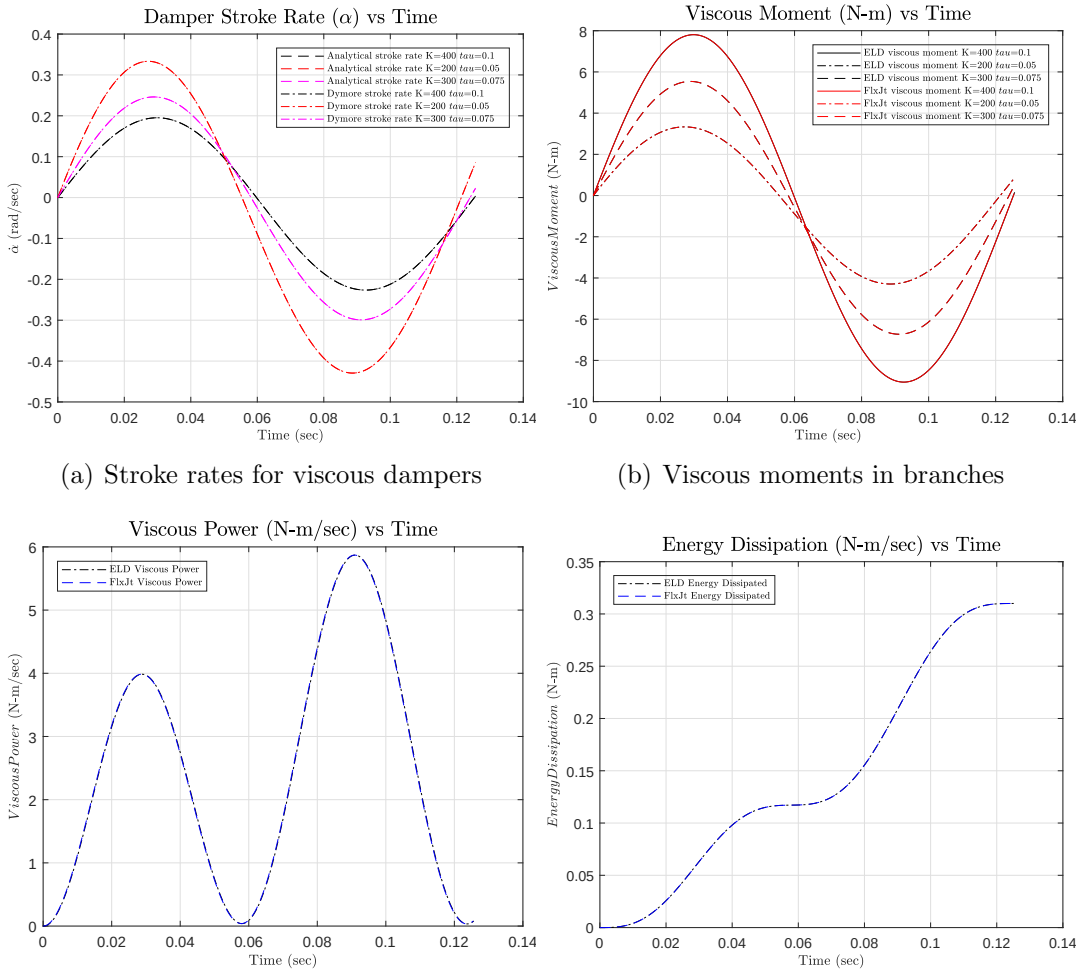

(a) Stroke rates for viscous dampers

(b) Viscous moments in branches

(c) Viscous power

(d) Energy dissipation

Fig. 5.6: Validation of quantities for an elastomeric damper element with a flexible joint element.

5.3 Tip loaded cantilever beam with homogeneous cross section

5.3.1 Problem statemant

The final application of viscoelastic material properties we look to investigate is for the case of elastic beams. The standard procedure for dealing with such problems is using a full scale three dimensional model. However the approach is very time consuming. A novel approach for the purpose of investigating such problems

is presented in [1]. The basic idea is to reduce the full scale three dimensional problem into a two-dimensional cross sectional analysis problem and thereafter a one dimensional elastic beam problem along the length of the beam. The approach for resolving the effects of viscoelasticity is similar to the problems solved earlier. The only difference is that we are looking to solve for the curvature in the beam at every time step instead strains or displacements. The beam model that was used is presented in fig. 5.7. The beam we have considered is 0.5m in length ans the cross sectional dimensions are 0.05 m and 0.0375 m. A time varying sinusoidal force is applied at the tip of the beam with an amplitude of 100 N and a time period of 0.6 sec. The model was validated with the help of full scale three dimensional finite element models built using ANSYS.

Fig. 5.7: Tip loaded cantilever beam modelled in Dymore.

5.3.2 Cross sectional properties and finite element model

The first case we look at is that of a beam with a homogeneous viscoelastic cross section. The Young's modulus for the elastic section is $1.456 * 10^{10} N/m^2$. The sectional matrices obtained using section builder for the elastic branch was

$$\underline{\underline{C_\infty}} = \begin{bmatrix} 2.730 * 10^7 & & & & & \\ & 8.731 * 10^6 & & & & \\ & & 8.607 * 10^6 & & & \\ & & & 2.665 * 10^3 & & \\ & & & & 3.199 * 10^3 & \\ & & & & & 5.687 * 10^3 \end{bmatrix} \tag{5.25}$$

A quick sanity check for the obtained matrix would be to check the value of the term $\underline{\underline{C_\infty}}_{55}$ which should be the same as the bending stiffness, H^{33} of the beam. The off-diagonal terms are small. The subsequent sectional stiffness matrices for the viscous branches are easily obtained as the damping ratio times the given matrix for the simple case of a homogeneous viscoelastic cross section. Two cases of one and three viscoelastic branches are considered. The model consisting of one branch has a damping ratio, $\mu_1 = 0.4$ and a relaxation time $\tau_1 = 0.1\,\text{sec}$ whereas the model consisting of three branches has damping ratios $\mu_1 = 0.025$, $\mu_2 = 0.05$ and $\mu_3 = 0.075$ and relaxation times $\tau_1 = 0.1$ *sec*, $\tau_2 = 0.05$ *sec* and $\tau_3 = 0.075$ *sec*. For the purpose of cross sectional analysis the model has 8 and 6 elements in the cross-sectional dimensions. For the beam problem we have 80 third order elements along the length. For the three dimensional analysis using ANSYS we have brick elements of $6.25 * 10^{-3} m$ in all dimensions which makes a total of 3840 elements of the 20 node SOLID186 type.

	ANSYS	Dymore	% error
Frequency (Hz)	1.6312	1.6351	0.24
Amplitude (mm)	1.1915	1.2098	1.54

Tab. 5.1: FFT analysis for one viscoelastic branch

	ANSYS	Dymore	% error
Frequency (Hz)	1.6312	1.6316	0.02
Amplitude (mm)	1.1915	1.2400	4.07

Tab. 5.2: FFT analysis for three viscoelastic branches

5.3.3 Results

The tip displacements were compared for ANSYS & Dymore. A good comparison of the results is seen for the different cases. An FFT analysis of the tip displacements was done and the dominant frequency and its amplitude are presented in tables 5.1 & 5.2. The frequencies show very good correlation, however the amplitudes do not show the same quality of agreement. It can be attributed to the quantity of damping present in the beam. This phenomenon will be clarified in the subsequent example.

5.3.4 Computational efficiency

Using the sectional stiffness matrices coupled with a one dimensional solution for dealing with the beam dynamics can give us to significant gains in computational efficiency. The solution time for different approaches is is given in table 1.

Cross section	3-D FEM	SectionBuilder and Dymore
1 branch homogeneous viscoelastic	2hr 52mins	21.89 sec
3 branches homogeneous viscoelastic	3hr 24mins	35.53 sec

Tab. 5.3: Solution times for the different computational approaches

5.4 Tip loaded cantilever beam with composite section

5.4.1 Problem statement

In structural components viscoelastic layers are added as a sandwich layer as a source of damping. In this section we consider a tip loaded cantilever beam made out of aluminum with a sandwich layer of viscoelastic rubber in between. A representative diagram of the same is shown in the fig. 5.8

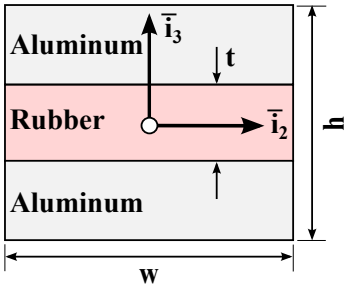

Fig. 5.8: Cross sectional representation of sandwich composite beam.

The external dimensions of the beam and its cross section are the same as the homogeneous cross-section considered previously. The beam now consists of a viscoelastic rubber layer sandwiched between two layers of aluminum, each having a thickness, t of 0.0125 m. The material properties of the aluminum and viscoelastic rubber layers consisting of a single viscous Maxwell fluid branch used for the section are given table 5.4.

Property	Aluminum	Viscoelastic rubber
Young's modulus (GPa)	73	20
Poisson's ratio	0.3	0.42
Material density (kg/m^3)	2770	1000
Damping ratio (μ)	N/A	0.01, 0.02, 0.05, 0.1
Relaxation time (sec)	N/A	0.1

Tab. 5.4: Solution times for the different computational approaches

μ	$\sigma_{11,max}(Pa)$	$\sigma_{11}^{error}(Pa)$	$\sigma_{11}^{error}(\%)$	$\sigma_{11}^{v,max}/\sigma_{11}^{e,max}(\%)$
0.01	164200	22.3373	0.0136	0.7299
0.02	165160	108.1643	0.0655	1.4596
0.05	168020	352.0861	0.2096	3.6498
0.1	172800	794.7212	0.4599	7.3044

Tab. 5.5: σ_{11} solutions obtained for various viscoelastic damping ratios.

5.4.2 Results

We would like to predict the stresses at any given point of the beam cross section using the formulation we have developed. This entails using the recovery relationships and the solution of the stress evolution equation described in previous sections. For as long as the recovery relationships work robustly, our formulation allows us to accurately evaluate both the elastic and viscous stresses in the rubber, a feature that is not commonly found in most commercial codes. This feature can be particularly useful when we look to model viscoelasticity for real world application, for example in case a specific level of damping is required for any application, having done this we can experimentally work backwards and select the appropriate viscoelastic material. For the given problem, the total stress results were obtained using the evolution equation and they are compared with the results obtained using the fully three dimensional finite element analysis done using ANSYS. With this study our target is to develop a measure of viscoelasticity which can be accurately modeled using the recovery relationships.

For the given cross-section various values of the viscoelastic damping ratio were considered and the solutions for stresses, σ_{11}, σ_{22} and τ_{13}, were obtained at different span-wise locations, η equal to 0.25, 0.50 and 0.75. The other three stress

μ	ANSYS	DYMORE	Error (%)
0.01	162322	162190	0.08
0.02	163240	163030	0.13
0.05	166008	165570	0.26
0.1	170682	169876	0.47

Tab. 5.6: FFT results for σ_{11} solutions.

μ	$\tau_{13}^{max}(Pa)$	$\tau_{13}^{error}(Pa)$	$\tau_{13}^{error}(\%)$	$\tau_{13}^{v,max}/\tau_{13}^{e,max}(\%)$
0.01	71812	607.0571	0.8453	0.7308
0.02	71806	810.3594	1.1285	1.4618
0.05	71771	1438.490	2.0043	3.6558
0.1	71734	2470.052	3.4433	7.2912

Tab. 5.7: τ_{13} solutions obtained for various viscoelastic damping ratios.

μ	ANSYS	DYMORE	Error (%)
0.01	70470	71034	0.80
0.02	70460	71232	1.10
0.05	70428	71826	1.99
0.1	70374	72822	3.48

Tab. 5.8: FFT results for τ_{13} solutions.

μ	$\sigma_{22}^{max}(Pa)$	$\sigma_{22}^{error}(Pa)$	$\sigma_{22}^{error}(\%)$	$\sigma_{22}^{v,max}/\sigma_{22}^{e,max}(\%)$
0.01	16919	179.6451	1.0618	0.7299
0.02	17086	257.5153	1.5072	1.4596
0.05	17574	478.7824	2.7244	3.6498
0.1	18389	851.5489	4.6308	7.3044

Tab. 5.9: σ_{22} solutions obtained for various viscoelastic damping ratios.

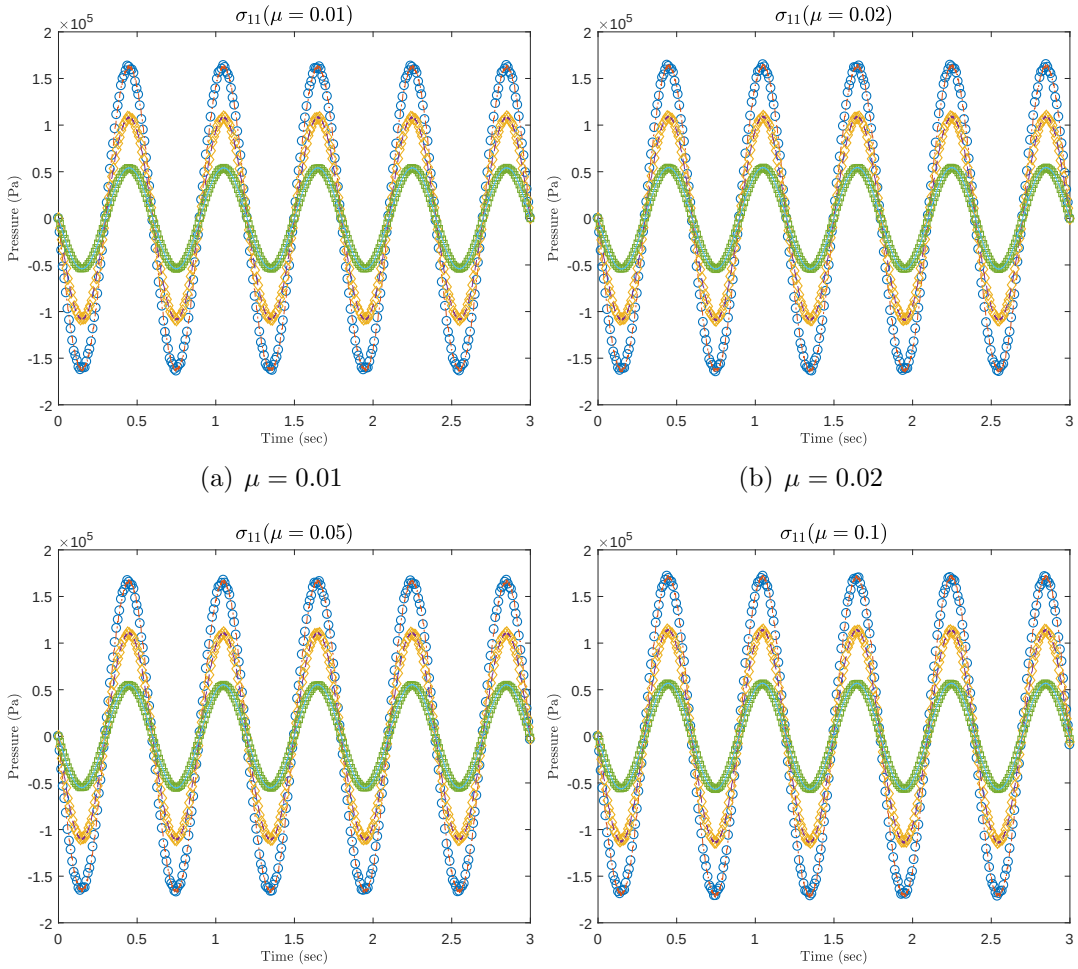

(a) $\mu = 0.01$ (b) $\mu = 0.02$

(c) $\mu = 0.05$ (d) $\mu = 0.10$

Fig. 5.9: σ_{11} at various span-wise locations of the beam where the DYMORE results and the respective symbols are $\eta = 0.25$ ($\bigcirc$), $\eta = 0.50$ ($\diamond$), $\eta = 0.75$ ($\square$) while the ANSYS results are generated using continuous lines using $\eta = 0.25$ ($-\bullet$), $\eta = 0.50$ ($--$), $\eta = 0.75$ ($-$)

μ	ANSYS	DYMORE	Error (%)
0.01	16724	16536	1.12
0.02	16884	16622	1.55
0.05	17368	16880	2.81
0.1	18176	17320	4.71

Tab. 5.10: FFT results for σ_{22} solutions.

solutions were negligible and are not shown. The stress solutions obtained are given in fig. 5.9, 5.10 and 5.11. The solutions compare favorably with the results obtained

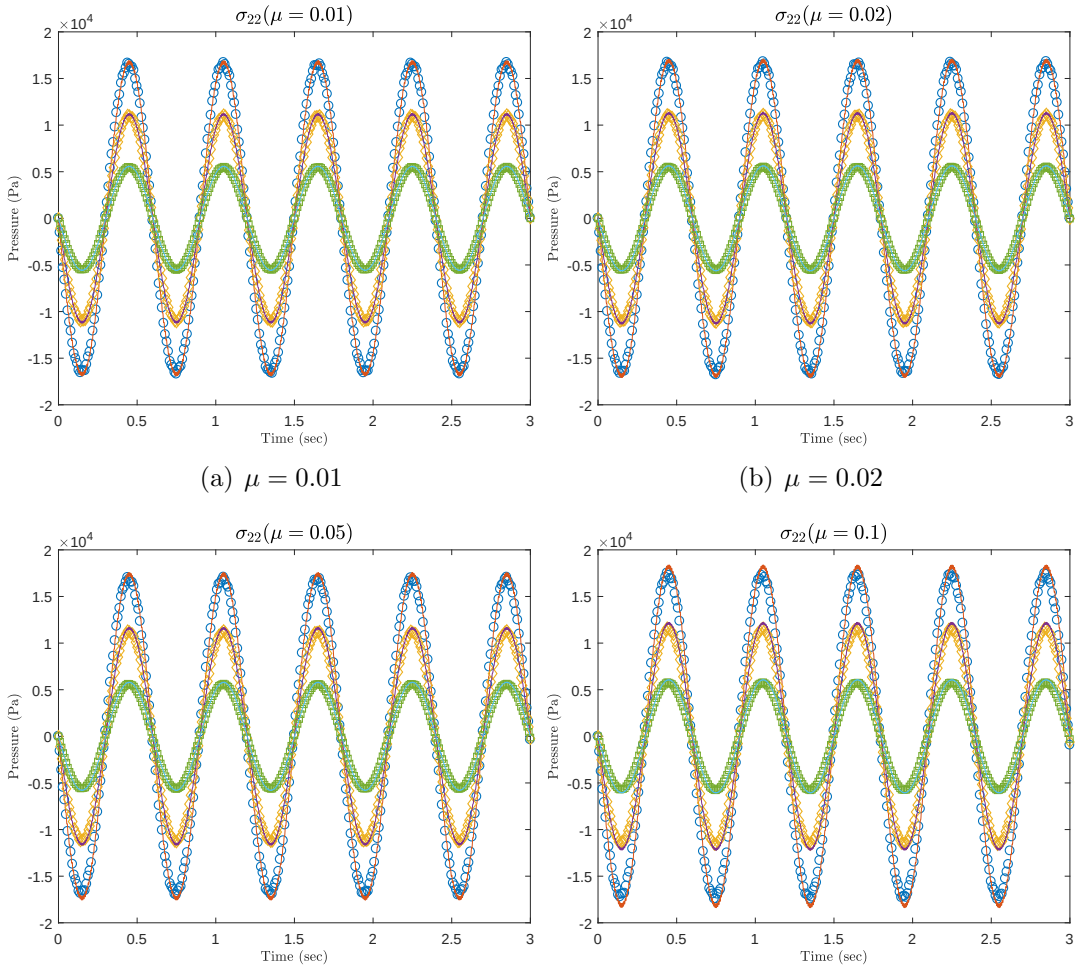

(a) $\mu = 0.01$ (b) $\mu = 0.02$

(c) $\mu = 0.05$ (d) $\mu = 0.10$

Fig. 5.10: σ_{22} at various span-wise locations of the beam where the DYMORE results and the respective symbols are $\eta = 0.25$ ($\bigcirc$), $\eta = 0.50$ ($\diamond$), $\eta = 0.75$ ($\square$) while the ANSYS results are generated using continuous lines using $\eta = 0.25$ ($-\bullet$), $\eta = 0.50$ ($--$), $\eta = 0.75$ ($-$)

using fully three dimensional finite element solutions. Naturally, the normal stress σ_{11} at a span-wise location closest to the fixed end would be the most critical. The maximum of the three stresses σ_{11}, σ_{22} and τ_{13} are presented in tables 5.5, 5.7 and 5.9. The percentage errors along with the proportion of viscoelastic stress to the elastic stress increases as the damping ratio is increased. The errors on the normal stress σ_{11} are extremely small, less than one percent, as presented in table 5.5. Since,

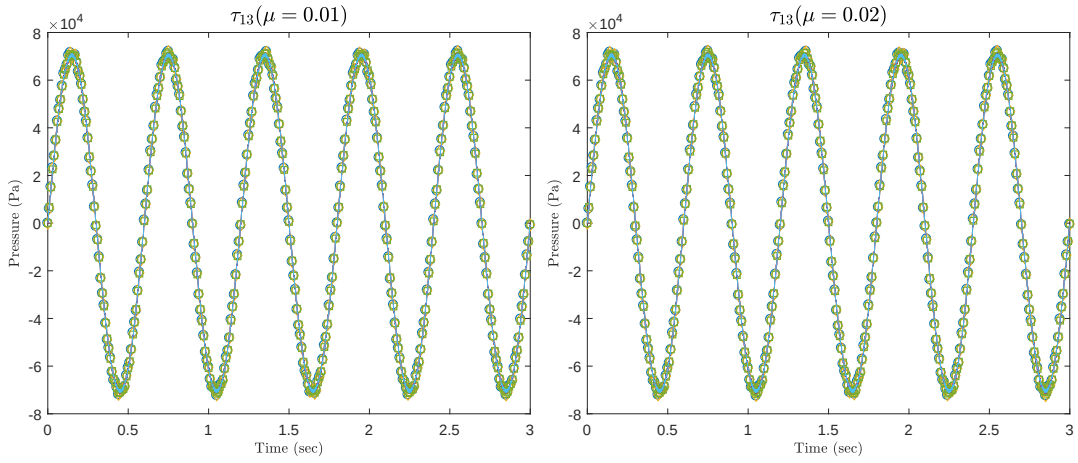

(a) $\mu = 0.01$ (b) $\mu = 0.02$

(c) $\mu = 0.05$ (d) $\mu = 0.10$

Fig. 5.11: τ_{13} at various span-wise locations of the beam where the DYMORE results and the respective symbols are $\eta = 0.25$ ($\bigcirc$), $\eta = 0.50$ ($\diamond$), $\eta = 0.75$ ($\square$) while the ANSYS results are generated using continuous lines using $\eta = 0.25$ ($-\bullet$), $\eta = 0.50$ ($--$), $\eta = 0.75$ ($-$)

values of viscous stresses as high as seven percent of elastic stresses are rarely, if at all found real structural materials, simulations for higher values of damping ratios are not presented. We also look to avoid the end effects in our solutions, hence they are obtained at a safe distance away from the fixed end. Finally an FFT analysis of the stress responses presented in tables 5.6, 5.8 and 5.10 was done. All the results

5.5 Hydraulic line reinforced with steel wires

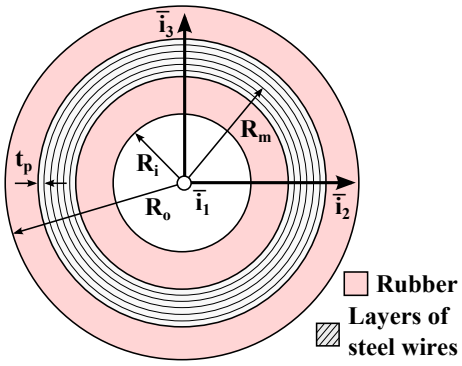

Fig. 5.12: Cross-sectional representation of the hydraulic line.

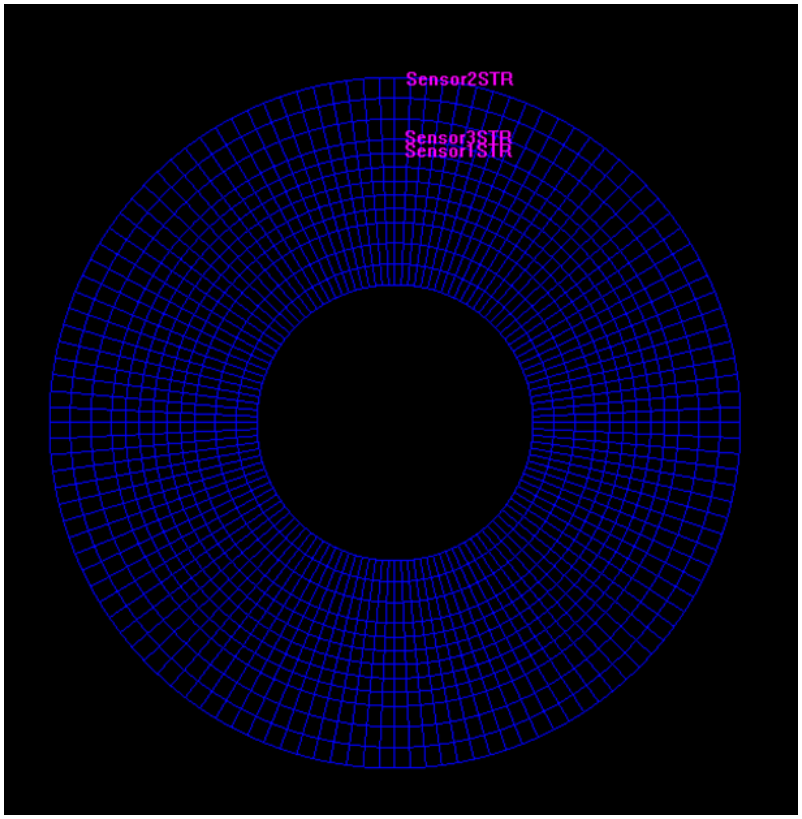

Fig. 5.13: Location of sensors on hydraulic line.

Having established the robustness of the proposed approach, we look to extend the application to the problem of a hydraulic line reinforced with six layers of steel wires. Such cross sections are generally found in heavy mechanical equipment The

tube has a inner and outer radii, R_i and R_o, of 10 mm and 25 mm respectively and a mean radius, R_m equal to $(R_i+R_o)/2$. Each layer of steel wire has a thickness t_p equal to 1 mm and they are wound around the tube at alternating $\pm 45^o$ angles. The material properties properties of the steel wires and the viscoelastic rubber are presented in table 5.11.

Property	Steel wires	Viscoelastic rubber
Longitudinal Young's modulus (GPa)	126	0.01
Transverse Young's modulus (GPa)	10	0.01
Poisson's ratio	0.38 $(\nu_{13} = \nu_{12})$, 0.3 (ν_{23})	0.42
Shear modulus (GPa)	8	0.0035
Material density (kg/m^3)	2770	1000
Relaxation time (sec)	N/A	0.1

Tab. 5.11: Material properties for the hydraulic line

μ	(I) $max(\sigma_{11}^{rub,e})$	(II) $max(\sigma_{11}^{rub,v})$	(III) $max(\sigma_{11}^{rub,t})$	(IV) $max(\sigma_{11}^{stl,e})$	(V) $max(\sigma_{11}^{stl,e}) - max(\sigma_{11\|\mu=0.01}^{stl,e})$	(VI) $max(\sigma_{11}^{rub,t}) - max(\sigma_{11\|\mu=0.01}^{rub,t})$
0.01	3273.560	24.154	3297.714	7503304	0.00E+00	0.00E+00
0.02	3273.509	48.308	3321.817	7503186	-1.18E+02	18.2697
0.05	3273.350	120.768	3394.118	7502823	-4.81E+02	73.0781
0.1	3273.091	241.533	3514.624	7502226	-1.08E+03	165.2290

Tab. 5.12: Stress results for the hydraulic line

5.5.1 Results

The locations where stress measurements are made are presented in fig. 5.13. "Sensor1STR" and "Sensor3STR" are placed over the steel wires while "Sensor2STR" were placed on the viscoelastic rubber, all the results were obtained at one-fourth span-wise distance from the root of the beam. The results for the maximum axial stresses in bending are presented in table 5.12. Columns (I) to (VI) present the maximum stresses in the various sensors, (I) is the maximum elastic stress at

"Sensor2STR", (II) the maximum viscous stress at "Sensor2STR", (III) the total stress at "Sensor2STR", (IV) the maximum stress at "Sensor3STR" and columns (V) and (VI) the difference of the total stresses on the sensors "Sensor2STR" and "Sensor3STR" from the values of stress obtained for damping ratio $\mu = 0.01$. The validity of the results can be simply analyzed by observing the increments in the viscous rubber and the steel wires respectively. From a basic understanding of solid mechanics we know that the total bending moment at the span-wise location should be a constant. Hence the integral sum of the moments produced by these internal stresses about the neutral axis over the cross section of the beam should be a constant. We find that while the overall change in the total stress in the steel wires is much higher than in case of rubber, a larger proportion of the rubber is present over the cross-section and is associated with larger moment arms.

Chapter 6: Future Work

6.1 Introduction & Assumptions

The formulations presented in the previous sections can be leveraged to set up a simple experiment that can be used to study viscoelasticity in beams. We look to set up a simple beam experiment with a uniform cross-section to simulate viscoelastic behavior experimentally. We have to keep in mind that the assumptions made previously continue to apply, ie. we are working with low damping & low frequency problems. This in turn implies that we are dealing with problems where viscous stresses & warping motions are small. These assumptions are reasonable for for modeling an Euler-Bernoulli(EB) beam as well. The main kinematic assumptions associated with an EB beam are that the cross-section is infinitely rigid in its own plane, the cross-section of a beam remains plane after deformation and the cross-section remains normal to the deformed axis of the beam [26].

6.2 Experimental Setup

A relevant objective of such an experiment can be to determine viscoelastic bending stiffness of a material. The simplest type of experiment, the four point

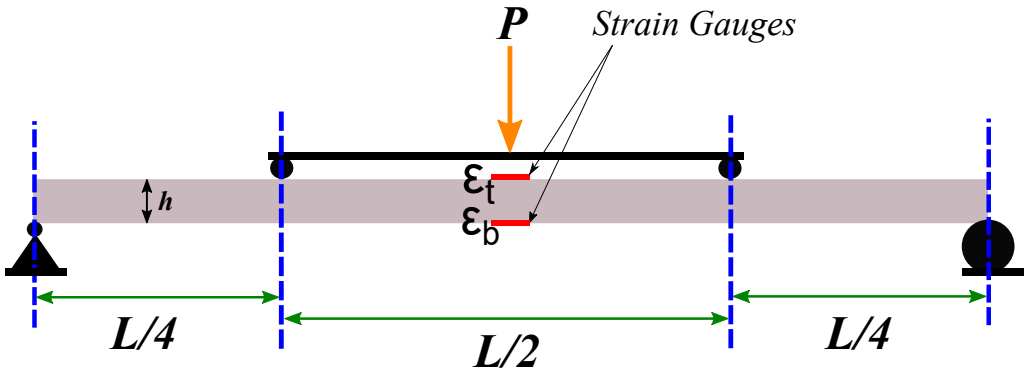

Fig. 6.1: Four point bending test diagram

bending experiment, to study bending in beams is considered. The four point bending experiment is based on the Euler Bernoulli beam theory as given in [26]. This is reasonable based on the assumptions we made to model viscoelasticity using the three dimensional beam theory in [20]. An experimental setup similar to fig. 6.1 can be set up. We consider a simply supported beam with a homogeneous viscoelastic cross section having a single M.F. branch. We assume that the elastic bending stiffness of the material, H^e_{33}, & the relaxation time, τ^ν, associated with the M.F. branch are known. These can be determined from quasi-static tests. The relaxation time for a viscoelastic material is defined as the time in which the instantaneous stress $\sigma(t)$ reduced to 37% of the initial stress σ_0 [27]. Having done this the four point bending experiment will have to be set up as shown in fig 6.1. A dynamic, time varying, preferably periodic load, P can be applied to the beam. The time varying strains ε_b & ε_t are to be recorded to evaluate the total curvature, κ^t using eq. 6.1.

$$\kappa^t = \frac{\varepsilon_b - \varepsilon_t}{h} \tag{6.1}$$

The instantaneous internal states, β^{ν}, can now be determined using the evolution equation as shown in eq. 6.2.

$$\tau^{\nu}\dot{\beta^{\nu}} + \beta^{\nu} = \kappa^{t} \tag{6.2}$$

Finally, using the known applied moment the viscoelastic bending stiffness can be measured using eq.6.3.

$$M = H_{33}^{e}\kappa^{t} + H_{33}^{v}(\kappa^{t} - \beta^{\nu}) \tag{6.3}$$

Chapter 7: Conclusion

A solution procedure for the analysis of viscoelastic beams and joints was presented for the generalized Maxwell model of viscoelasticity. The method was integrated with flexible multi body dynamics solution techniques. The response observed in joints showed an exact comparison with analytical solutions. For the case of beams using a sectional level approach it was shown that robust results can be obtained for complex cross sections. Lastly while running the analysis for beams it was shown that the it must comply with the basic assumptions made in order to implement these simplifications. The first being that the structure being studied is subjected to low frequency excitations. The second being that the damping forces encountered should be low. Both assumptions are valid for most practical problems, particularly structural problems in aerospace engineering. It is understood that wherever these conditions are not met, the given problem should be treated as a fully three dimensional one instead. A practical example of a hydraulic line with viscoelastic rubber was presented and the cross sectional analysis for the same was done.

Bibliography

[1] V. Giavotto, M. Borri, P. Mantegazza, G. Ghiringhelli, V. Carmaschi, G.C. Maffioli, and F. Mussi. Anisotropic beam theory and applications. *Computers & Structures*, 16(1-4):403–413, 1983.

[2] J.C. Simo, K.D. Hjelmstad, and R.L. Taylor. Numerical formulations of elasto-viscoplastic response of beams accounting for the effect of shear. *Computer Methods in Applied Mechanics and Engineering*, 42(3):301–330, 1984.

[3] P. Mata, S. Oller, and A.H. Barbat. Dynamic analysis of beam structures considering geometric and constitutive nonlinearity. *Computer Methods in Applied Mechanics and Engineering*, 197(6-8):857–878, 2008.

[4] J.C. Simo. A finite strain beam formulation. The three-dimensional dynamic problem. Part I. *Computer Methods in Applied Mechanics and Engineering*, 49(1):55–70, 1985.

[5] A.M. Abdel-Nasser and A.A. Shabana. A nonlinear viscoelastic constitutive model for large rotation finite element formulations. *Multibody System Dynamics*, 26(3):57–79, 2011.

[6] S.S. Antman. Invariant dissipative mechanisms for the spatial motion of rods suggested by artificial viscosity. *Journal of Elasticity*, 70:55–64, 2003.

[7] N.M. Ribe. Coiling of viscous jets. *Proceedings of the Royal Society of London, Series A*, 460(2051):3223–3239, 2004.

[8] F.T. Trouton. On the coefficient of viscous traction and its relation to that of viscosity. *Proceedings of the Royal Society of London, Series A*, 77:426–440, 1906.

[9] S. Panda, N. Marheineke, and R. Wegener. Systematic derivation of an asymptotic model for the dynamics of curved viscous fibers. *Mathematical Methods in the Applied Sciences*, 31:1153–1173, 2008.

[10] N. Marheineke and R. Wegener. Asymptotic model for the dynamics of curved viscous fibers with surface tension. *Journal of Fluid Mechanics*, 622:345–369, 2009.

[11] A. Klar, N. Marheineke, and R. Wegener. Hierarchy of mathematical models for production processes of technical textiles. *Zeitschrift für angewandte Mathematik und Mechanik*, 89(12):941–961, 2009.

[12] W. Arne, N. Marheineke, J. Schnebele, and R. Wegener. Fluid–fiber interaction in rotational spinning process of glass wool production. *Journal of Mathematics in Industry*, 1(2), 2011.

[13] H. Lang, J. Linn, and M. Arnold. Multibody dynamics simulation of geometrically exact Cosserat rods. *Multibody System Dynamics*, 25(3):285–312, 2011.

[14] M. Schulze, S. Dietz, B. Burgermeister, A. Tuganov, H. Lang, J. Linn, and M. Arnold. Integration of nonlinear models of flexible body deformation in multibody system dynamics. *Journal of Computational and Nonlinear Dynamics*, 9(1):011012, 2013.

[15] H. Lang, S. Leyendecker, and J. Linn. Numerical experiments for viscoelastic Cosserat rods with Kelvin–Voigt damping. In *Proceedings of the ECCOMAS Thematic Conference Multibody Dynamics, edited by by Z. Terze and M. Vrdoljak*, pages 453–462, 2013.

[16] J. Linn, H. Lang, and A. Tuganov. Geometrically exact Cosserat rods with Kelvin-Voigt type viscous damping. *Mechanical Sciences*, 4:79–96, 2013.

[17] G.R. Cowper. The shear coefficient in Timoshenko's beam theory. *Journal of Applied Mechanics*, 33:335–340, 1966.

[18] W. Flügge. *Viscoelasticity*. Springer-Verlag, New York, Berlin, second revised edition, 1975.

[19] J.D. Ferry. *Viscoelastic Properties of Polymers*. Wiley, New York, second edition, 1970.

[20] O.A. Bauchau and S.L. Han. Three-dimensional beam theory for flexible multibody dynamics. *Journal of Computational and Nonlinear Dynamics*, 9(4):041011 (12 pages), 2014.

[21] O.A. Bauchau. *Flexible Multibody Dynamics*. Springer, Dordrecht, Heidelberg, London, New-York, 2011.

[22] S.L. Han and O.A. Bauchau. Nonlinear three-dimensional beam theory for flexible multibody dynamics. *Multibody System Dynamics*, 34(3):211–242, July 2015.

[23] O.A. Bauchau and S.L. Han. Flexible joints in structural and multibody dynamics. *Mechanical Sciences*, 4(1):65–77, 2013.

[24] V.V. Volovoi, D.H. Hodges, V.L. Berdichevsky, and V.G. Sutyrin. Dynamic dispersion curves for non-homogeneous, anisotropic beams with cross sections of arbitrary geometry. *Journal of Sound and Vibration*, 215:1101–1120, 1998.

[25] S.L. Han and O.A. Bauchau. Nonlinear, three-dimensional beam theory for dynamic analysis. *Multibody System Dynamics*, 41(2):173–200, 2017.

[26] O.A. Bauchau and J.I. Craig. *Structural Analysis with Application to Aerospace Structures*. Springer, Dordrecht, Heidelberg, London, New-York, 2009.

[27] G.C. Papanicolaou and S.P. Zaoutsos. 1 - viscoelastic constitutive modeling of creep and stress relaxation in polymers and polymer matrix composites. In Rui Miranda Guedes, editor, *Creep and Fatigue in Polymer Matrix Composites (Second Edition)*, Woodhead Publishing Series in Composites Science and Engineering, pages 3 – 59. Woodhead Publishing, second edition edition, 2019.